Geoscience Frontiers xxx (2016) 1–19

HOSTED BY

ELSEVIER

Contents lists available at ScienceDirect

China University of Geosciences (Beijing)

Geoscience Frontiers

journal homepage: www.elsevier.com/locate/gsf

Research paper

Modulation of ice ages via precession and dust-albedo feedbacks

Ralph Ellis [a,*], Michael Palmer [b]

[a] 105 – 6817 Route Pommier, St Martin Bellevue 74370, France
[b] University of Waterloo, Department of Chemistry, Waterloo, Ontario, Canada

ARTICLE INFO

Article history:
Received 23 March 2016
Received in revised form
17 April 2016
Accepted 30 April 2016
Available online xxx

Keywords:
Paleoclimatology
Ice-age
Precession
CO_2
Albedo
Dust

ABSTRACT

We present here a simple and novel proposal for the modulation and rhythm of ice-ages and interglacials during the late Pleistocene. While the standard Milankovitch-precession theory fails to explain the long intervals between interglacials, these can be accounted for by a novel forcing and feedback system involving CO_2, dust and albedo. During the glacial period, the high albedo of the northern ice sheets drives down global temperatures and CO_2 concentrations, despite subsequent precessional forcing maxima. Over the following millennia more CO_2 is sequestered in the oceans and atmospheric concentrations eventually reach a critical minima of about 200 ppm, which combined with arid conditions, causes a die-back of temperate and boreal forests and grasslands, especially at high altitude. The ensuing soil erosion generates dust storms, resulting in increased dust deposition and lower albedo on the northern ice sheets. As northern hemisphere insolation increases during the next Milankovitch cycle, the dust-laden ice-sheets absorb considerably more insolation and undergo rapid melting, which forces the climate into an interglacial period. The proposed mechanism is simple, robust, and comprehensive in its scope, and its key elements are well supported by empirical evidence.

1. Introduction

Since the discovery of ice-age cycles almost two centuries ago, a large amount of geological evidence has been assembled from a variety of sources, and many different hypotheses have been advanced to account for their approximate 100 kyr periodicity and asymmetric, saw-tooth temperature response. Improved calculations of Milankovitch insolation cycles and greater precision of Antarctic ice-core records demonstrate that each major deglaciation coincides with maximum summer insolation in the northern hemisphere. And yet many of the other insolation maxima only trigger minor warming events, and so interglacials only occur after four or five insolation cycles. No generally accepted explanation exists for this peculiar intermittent climate response, and any comprehensive explanation for ice-age modulation and periodicity has to be able to explain this anomaly.

The answer to this conundrum can be found in a novel reanalysis of the effects of decreasing atmospheric CO_2 concentrations during an ice-age. Ice age CO_2 reductions coincide with an increase in ice sheet extent and therefore an increase in global albedo, and this should result in further cooling of the climate. But what actually happens is that when CO_2 reaches a minimum and albedo reaches a maximum, the world rapidly warms into an interglacial. A similar effect can be seen at the peak of an interglacial, where high CO_2 and low albedo results in cooling. This counterintuitive response of the climate system also remains unexplained, and so a hitherto unaccounted for agent must exist that is strong enough to counter and reverse the classical feedback mechanisms.

The answer to both of these conundrums lies in glacial dust, which was deposited upon the ice sheets towards the end of each glacial maximum. Previous research has considered two effects of this aeolian dust on the glacial climate: the increased albedo of atmospheric dust cooling the climate, and the mineral fertilization of marine life reducing atmospheric CO_2. But both of these effects would result in a cooling feedback, and therefore provide no

Abbreviations: NH, Northern hemisphere; SH, Southern hemisphere; CGY, Celestial Great Year averaging 25,700 years (caused by precession); SGY, Seasonal Great Year averaging 22,200 years (including apsidal precession); ESS, Earth System Sensitivity; ECS, Equilibrium Climate Sensitivity; YD, Younger Dryas; ITCZ, Inter-Tropical Convergence Zone; ISA, International Standard Atmosphere; ICAO, International Civil Aviation Organisation; MPT, Mid-Pleistocene Transition; PMIP, Paleoclimate Modeling Intercomparison Project; amsl, above mean sea level; TSI, Total Solar Irradiance; D-O, Dansgaard-Oeschger warming event.

* Corresponding author.
E-mail address: ralph.ellis@me.com (R. Ellis).

Peer-review under responsibility of China University of Geosciences (Beijing).

http://dx.doi.org/10.1016/j.gsf.2016.04.004

Please cite this article in press as: Ellis, R., Palmer, M., Modulation of ice ages via precession and dust-albedo feedbacks, Geoscience Frontiers (2016), http://dx.doi.org/10.1016/j.gsf.2016.04.004

explanation for the interglacial warming that appears to result from dust deposition. In great contrast to these explanations it is proposed here that during the glacial maximum, CO_2 depletion starves terrestrial plant life of a vital nutrient and causes a die-back of upland forests and savannahs, resulting in widespread desertification and soil erosion. The resulting dust storms deposit large amounts of dust upon the ice sheets and thereby reduce their albedo, allowing a much greater absorption of insolation. Up to 180 W/m^2 of increased absorption can be provided to the northern ice sheets, when calculated seasonally and regionally instead of annually and globally.

This dramatic increase in insolation and absorption results in melting and dissipation of the northern ice sheets, and the establishment of a short interglacial period. Ice ages are therefore forced by orbital cycles and Milankovitch insolation, but regulated by ice-albedo and dust-albedo feedbacks. And the warming effects of dust-ice albedo are counterintuitively caused by a reduction in global temperatures and a corresponding reduction in CO_2 concentrations. And while this proposal represents a reversal of conventional thinking it does explain each and every facet of the glacial cycle, and all of the many underlying mechanisms that control its periodicity and temperature excursions and limitations.

2. Orbital forcing of ice-ages and interglacials

2.1. Late Pleistocene climatic cycles

The graph of ice-age temperature vs. CO_2 in Fig. 1 demonstrates that glacial cycles over the last 800 kyr display a quasi-100 kyr cycle that superficially mimics the Earth's approximately 100 kyr orbital eccentricity. To be more precise, recent ice-age cycles are either ~90 kyr or ~115 kyr in length, and this is a fundamentally important distinction as will be explained later. The precise agent, periodicity, and mechanism through which these late Pleistocene ice-ages have been modulated remains a contentious issue, and so the IPCC's 2014 AR5 report says of this scientific lacuna:

> *Orbital forcing is considered the pacemaker of transitions between glacials and interglacials (high confidence), although there is still no consensus on exactly how the different physical processes influenced by insolation changes interact to influence ice sheet volume.* (IPCC AR5 5.2.1.1. See also AR4 B6.1, FAQ 6.1)

It will be demonstrated shortly that the primary orbital cycle controlling paleoclimate over the last 800 kyr is precession, because the variations in regional insolation generated by this orbital cycle are demonstrably linked to interglacial warming. Yet this common assumption, which has been endorsed yet not fully explained by the IPCC, is by no means universally accepted. Huybers invoked axial obliquity as the controlling cycle (Huybers, 2006); Kirkby suggested cosmic ray flux (Kirkby et al., 2004); Muller championed orbital inclination (Muller and MacDonald, 1997); Lisiecki pointed towards an 'internally driven climate oscillation phase locked to eccentricity' (Lisiecki, 2010); while Liu introduced a 'pulse modulation' to the precessional cycle (Liu, 1998).

Because of these many competing theories, a short explanation of the precessional cycle and its effects on climate is required. And there is an obvious and frequently highlighted problem with invoking the precessionary cycle for glacial modulation, and that is the curious issue of the missing cycles in the climatic record. This has been a major stumbling block in all paleoclimatic research, because the reason for the climate displaying a selective response to orbital forcings has never been adequately explained. However, the missing precessionary cycle problem forms the very foundation of this thesis and so it will be comprehensively and conclusively accounted for.

2.2. Orbital cycles and forcing

There are three main orbital cycles that influence and regulate the intensity of terrestrial insolation in the high latitudes, and these are obliquity, eccentricity and precession. Although each of these cycles has a unique effect, it is the complex interplay between these orbital cycles that provides the insolation forcing for each ice age cycle:

Precession:

Precession describes the rotational motion of the Earth's axial orientation. Axial precession has a roughly 25.7 kyr cycle, and it was known to the ancient Egyptians, Greeks and Chinese as the Great Year (Yoke, 1985; Campion and Dally, 1997). And its comparison to an annual year is quite valid, because the Celestial Great Year combines with orbital eccentricity to produce warm and cool seasons in each hemisphere. However, apsidal precession reduces the approximate 25.7 kyr Celestial Great Year down to an approximate 23 kyr cycle, which will be called herein the 'Seasonal Great Year' (SGY). So each Great Season of this Seasonal Great Year is approximately 5700 years long, and this is a significant periodicity because most of the interglacial warming events last about 5000 years.

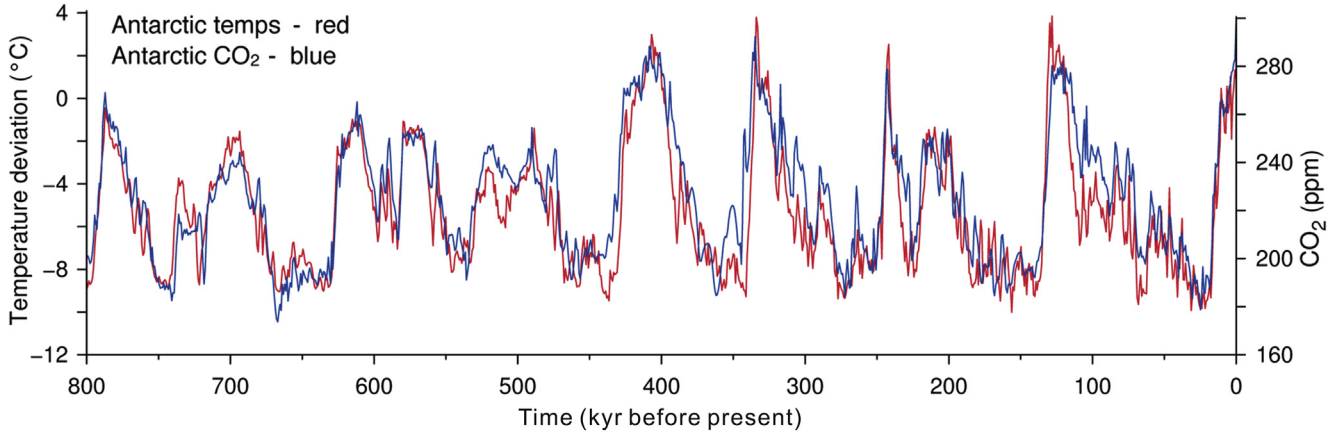

Figure 1. Antarctic temperature vs. CO_2 over 800 kyr from the Epica3 ice core. Note that CO_2 concentrations follow global temperatures very closely, giving the illusion of CO_2 being the primary causal feedback factor. Source: Epica3, 2007.

Please cite this article in press as: Ellis, R., Palmer, M., Modulation of ice ages via precession and dust-albedo feedbacks, Geoscience Frontiers (2016), http://dx.doi.org/10.1016/j.gsf.2016.04.004

These are average figures as the SGY has ranged from 15 kyr to 27 kyr over the last 400 kyr (Laskar et al., 2004), a variable cycle that is likely to generate confusion if specific numbers or averaged lengths of precessional cycles are assumed to be controlling the interglacial cycle.

Eccentricity:

Eccentricity describes the ellipticity of the Earth's orbit, which varies from a near-circular 0.002 to a maximum of 0.050 (IPCC AR4 B6.1). On its own eccentricity has no direct forcing potential whatsoever, providing just 0.4 W/m^2 of increased insolation over its entire 90–100 kyr cycle. And yet eccentricity does play a role in interglacial modulation because orbital eccentricity increases the potency of the SGY, resulting in periods of enhanced SGYs that follow the eccentricity cycle. This effect is clearly demonstrated Fig. 2, where northern Great Summers over 510 W/m^2 at midsummer (orange plot) have been banded with orange shading, and these enhanced SGYs clearly cluster together around the high eccentricity peaks (blue plot). And since these clusters of enhanced Great Summers can provide up to an extra 110 W/m^2 to the northern latitudes during each annual midsummer, it is not so surprising that they all line up with interglacial warming and the subsequent ice-age cycle, as depicted here by the red plot. And so the ghost of eccentricity can still be seen within the ice-age cycle, because it is eccentricity that dictates the strength of the Great Summer.

Obliquity:

Obliquity describes the angle of the Earth's axial inclination, which varies from 22.1° to 24.5° over an approximate 41 kyr cycle. The obliquity cycle can vary the insolation received in high northern latitudes by up to 25 W/m^2, or about a quarter of the variation normally produced by the precessionary cycle. However, during periods of low eccentricity when the SGY has very weak seasons, like 400 kyr ago in Fig. 2, obliquity can play a significant role in high latitude insolation and warming. This is why the insolation peak 340 kyr ago is greater than the peak 320 kyr ago, even though the latter had a greater precessionary index amplitude, because the former was in phase with the obliquity maximum while the latter was out of phase. Likewise, up to 40% of the increase in insolation for the interglacial periods 430 kyr ago and 15 kyr ago was provided by obliquity rather than precession, and so these interglacials were only successful because of obliquity assistance.

When acting in concert, these three orbital cycles are capable of substantially varying high latitude terrestrial insolation, a cyclical oscillation known as the Milankovitch Cycle after the Serbian astronomer who made the first calculations. The upper orange plot in Fig. 2 shows the variation in terrestrial Milankovitch insolation at 65°N over the last 450 kyr, with the peaks and troughs denoting Great Summers and Great Winters respectively. So although this plot is primarily following the precessionary SGY, its strength and effectiveness have been modulated by both obliquity and eccentricity. This is why researchers have sometimes seen the influence of obliquity or eccentricity within interglacial periodicity, because their effects can become apparent on some occasions.

While the precessional SGY will be shown to have been the primary forcing agent regulating ice ages since the Mid-Pleistocene Transition (MPT) 800 kyr ago, obliquity was dominant prior to this time. So while all three of these orbital cycles act in concert to modulate insolation at high latitudes, the resulting periodicity of ice ages and interglacials must also be regulated by terrestrial feedback factors. According to Laskar's orbital data, Milankovitch insolation strengths and periodicity have not changed significantly for millions of years (Laskar et al., 2004). And so if solar TSI is assumed to have been constant during the Pleistocene era, the noticeable shift from obliquity to precessional ice age modulation must have been triggered by changes in terrestrial feedback factors. The reason for this abrupt change lies beyond the scope of this paper, but its conclusions might suggest that the MPT and the many sudden D-O warming events were caused by changes in NH ice-sheets and their albedo. This will be the subject of a later paper.

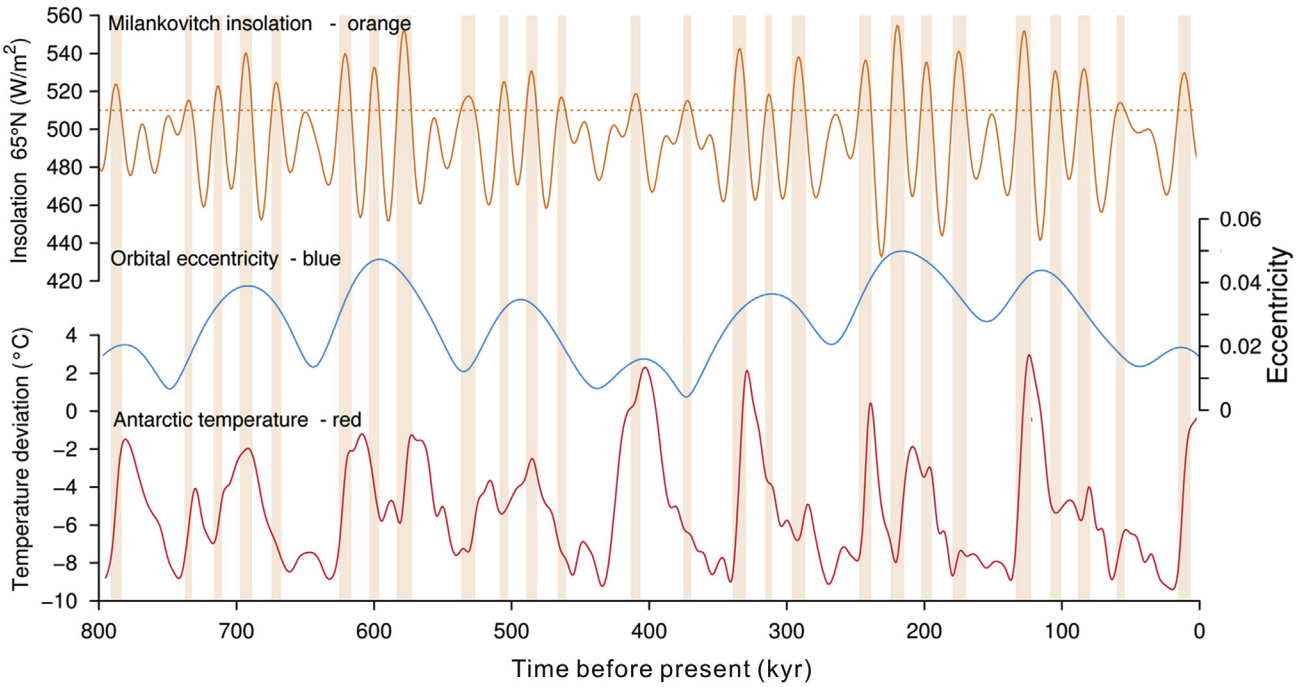

Figure 2. An illustration of why ice-ages follow the Earth's orbital eccentricity. Eccentricity-enhanced precessional Great Summers over 510 W/m^2 are marked with orange shading, and these clusters of shaded Great Summers are closely correlated with the ice-age cycle. Source: Laskar et al., 2004 orbital data. Epica3 Antarctic temperature data.

Please cite this article in press as: Ellis, R., Palmer, M., Modulation of ice ages via precession and dust-albedo feedbacks, Geoscience Frontiers (2016), http://dx.doi.org/10.1016/j.gsf.2016.04.004

Table 1
Seasonal Great Year cycle lengths vs. ice-age duration. The upper row represents the last ice-age, while subsequent rows progress back through previous glacial cycles.

SGY lengths (kyr)	Cluster length (kyr)	Ice-age duration (kyr)
23, 21, 26, 22, 25	117	117
23, 22, 23, 24, 23	115	115
21, 21, 27, 22	91	90
16, 22, 15, 17, 22	92	90
25, 20, 22, 17, 21	105	99

Ice ages are measured between glacial terminations. Source Laskar et al., 2004, Epica3. SGY lengths are measured between maximum insolation peaks. Left to right = older to younger.

2.3. Great Year modulation and clusters

The shaded bands in Fig. 2 demonstrate that the glacial cycle is coincident with clusters of precessional SGYs, and the last five clusters are presented in tabular form in Table 1. Each cluster in Table 1 contains four or five SGYs, guided by the ghost of eccentricity, and these clusters match with the temperature records in both Figs. 1 and 2.

This is confirmed by Fig. 3, which plots SGY Milankovitch insolation at 65°N (blue) vs. Antarctic temperatures (red). The five interglacial warmings and most of the minor warming events depicted here closely follow the insolation maximums, which represent the Great Summer season in the northern hemisphere. And so the primary astronomical metronome for late Pleistocene interglacial initiation involves a selective response to the SGY. Note that increasing temperatures never follow Great Summers in the southern hemisphere, represented here by the troughs in the insolation line. The likely reason is the northern hemisphere contains the great landmasses and the great ice-age ice sheets, which implies that landmasses and their attendant ice sheets are much more important than open oceans in interglacial initiation and propagation. And from this simple observation we might also propose that the primary forcing and feedback for interglacial modulation is likely to be albedo.

3. CO_2 and Albedo feedback mechanisms

3.1. The missing interglacial problem

The problem with invoking precessional Great Summers as the agent of interglacial warming, is that not all Great Summers have an effect, and so there must be another factor involved in ice-age modulation. In Fig. 2 the start of an enhanced cluster of Great Summers is always associated with the start of an interglacial period, presumably because the increased annual summer insolation over the full length of the 5700 year Great Summer provides an enormous amount of additional insolation directly to the northern ice sheets. In Fig. 3 the Holstein interglacial 340 kyr ago resulted in nearly 12 °C of warming, as measured in Antarctica, in about 5000 years. Yet the climate then cooled back into an ice-age, even though subsequent eccentricity-enhanced Great Summers in this cluster were equally strong as the first. So why did subsequent Great Summers not produce the same warming response? The strong Great Summer 170 kyr ago, for instance, failed to produce any warming response whatsoever.

The answer to this selective response must lie within the temperature feedback system. The primary feedback involved in modern terrestrial temperature feedbacks is said to be CO_2 (plus H_2O), and so it is assumed that CO_2 must also be closely involved in the interglacial warming process (Hansen et al., 2012). But there is a problem with this suggestion, because high CO_2 concentrations during an interglacial always result in cooling while low CO_2 concentrations during a glacial maximum always result in warming, as can be seen in Fig. 1. But if CO_2 was the primary feedback mechanism regulating glacial temperature responses, this is unlikely to happen in this fashion.

3.2. Albedo and CO_2 feedback strength

Hansen determined that between the LGM CO_2 concentration of 180 ppm and the pre-industrial concentration of 280 ppm, the extra feedback provided by CO_2 was about 2.25 W/m^2, which increases to about 3 W/m^2 when other factors are included (Hansen et al., 2012, Fig. 5c & p9). The IPCC data gives a similar figure of 2.8 W/m^2 for all greenhouse gases, but neither of these values include water vapour feedbacks (IPCC AR4 6.4.1.2, AR5 box 8.1 and Table 9.5). But since interglacial warming events average about 5000 years this represents just 0.006 W/m^2 per decade of additional feedbacks and warming, which is about a third of the energy required to power a honey bee in flight (Roberts and Elekonich, 2005).

The strength of the albedo feedback was calculated as being in the same range, or about 3 W/m^2 over the full interglacial cycle (Hansen et al., 2012, Fig. 5c and p12). This figure was derived by equating albedo with sea levels, and therefore with ice extent, which spreads the albedo effect out across the entire globe in a similar fashion to the calculation for CO_2. But this is likely to be an erroneous procedure. In the modern decadal world, the annual

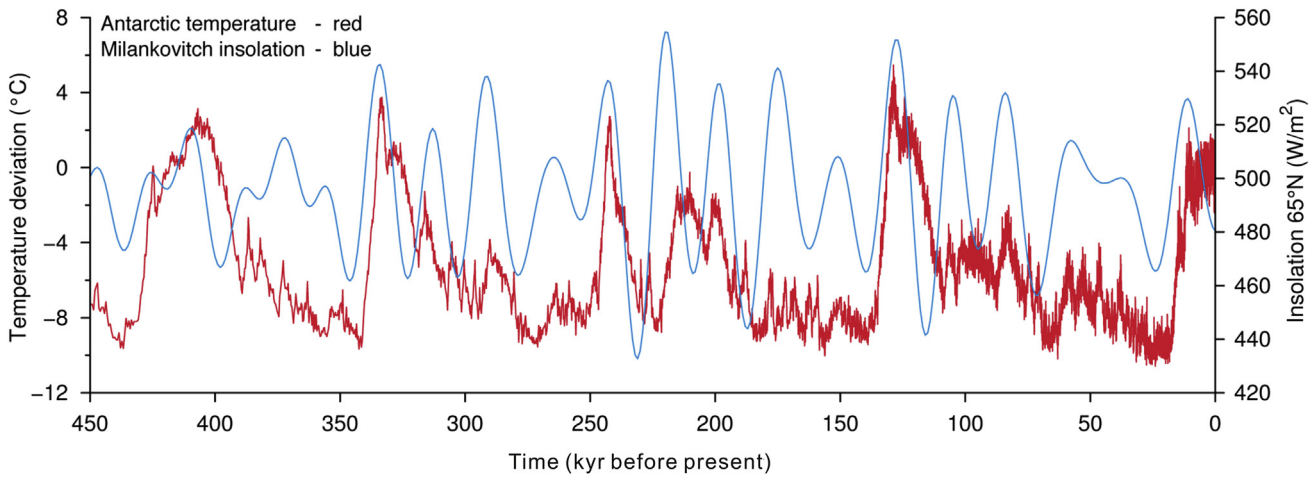

Figure 3. Graph of Milankovitch insolation at 65°N (blue) vs. Antarctic temperature (red). The graph plots the last 21 precessional Seasonal Great Years in W/m^2. The insolation peaks represent northern hemisphere Great Summer seasons, and the insolation troughs represent northern hemisphere Great Winter seasons. Sources: Laskar et al., 2004; Epica3, 2007.

Please cite this article in press as: Ellis, R., Palmer, M., Modulation of ice ages via precession and dust-albedo feedbacks, Geoscience Frontiers (2016), http://dx.doi.org/10.1016/j.gsf.2016.04.004

melting of snow and ice in Canada is caused by summer insolation and temperature increases in North America, rather than the ambient temperature in Argentina. Similarly, in the millennial ice-age world the warming of the northern ice sheets is likely to be a local and regional phenomena in the northern hemisphere during a Great Summer. As Fig. 3 clearly demonstrates, interglacials are only ever triggered by Great Summer insolation increases in the northern hemisphere and never by increases in insolation during the southern Great Summer, so why spread the influence of albedo across the entire globe?

In great contrast to the global averaging by Hansen, the regional influence of albedo absorption is very strong. Fig. 3 shows that annual midsummer insolation at 65°N during a Great Winter averages 450 W/m^2, and if 20% is deleted for cloud albedo then 360 W/m^2 of that insolation reaches the ground. But the snow covered higher latitudes might have an albedo of 0.90, which would mean that only 36 W/m^2 is being absorbed (Warren, 1984; Warren et al., 2009; Svensson et al., 2000, 2015). During a Great Summer the northern high latitude insolation rises to about 540 W/m^2, and the net insolation after cloud albedo is about 430 W/m^2, resulting in 43 W/m^2 absorption. So the change in high latitude insolation and absorption between the Great Winter and Great Summer is likely to be as shown in Table 2.

Table 2 demonstrates that the increase in insolation absorption between a Great Winter and Great Summer on reasonably clean ice sheets is only 7 W/m^2. This increase in insolation is not very significant, which is why some Great Summers only produce a small temperature response while others are ignored completely by the climate system. In order to generate a successful interglacial the increased insolation from a Great Summer needs to be enhanced, and the likely mechanism for this is dust contamination.

3.3. Reason for feedback limits

Another unexplained facet of the glacial cycle is the similar maximum interglacial temperatures, no matter how intense the Great Summer insolation. All the maximum interglacial temperatures in Fig. 3 are within 3 °C of each other, and since tropical temperature increases were about a third of polar increases, these interglacial periods must have all peaked within 1 °C of each other. So it would appear that there is another factor involved, which capable of regulating global temperatures to a set maximum during interglacials.

If CO_2 represented the primary feedback system during an interglacial, then the large rise in CO_2 concentrations could well produce a 'runaway greenhouse effect', a possibility that has been mentioned by many scientists including James Hansen (Hansen et al., 2011; Goldblatt, 2012; Goldblatt et al., 2014). And yet over the last five cycles, high CO_2 concentrations have resulted in global temperatures stabilising at about the same value, no matter how strong the Great Summer insolation. And this is despite CO_2 at the interglacial concentration of 280 ppm still having plenty of feedback potential left in it. However, in great contrast, an albedo feedback system driven by changes in polar ice extent will inevitably result in a maximum temperature limit, which is reached when the majority of the ice-sheets have melted and there are no further significant changes in ice-albedo to cause further feedbacks. And this is perhaps further evidence that the primary feedback in interglacial modulation is actually albedo, rather than CO_2.

Table 2
Difference in insolation and absorption during the Great Summer and Great Winter.

Great Winter (annual midsummer)	
Upper atmosphere insolation	450 W/m^2
Ice sheet insolation (less cloud)	360 W/m^2
Ice sheet absorption 0.90 albedo	36 W/m^2
Great Summer (annual midsummer)	
Upper atmosphere insolation	540 W/m^2
Ice sheet insolation (less cloud)	430 W/m^2
Ice sheet absorption 0.90 albedo	43 W/m^2
Absorption increase due Grt Summer	7 W/m^2

4. Effects of dust on albedo

4.1. Strength and sign of dust feedbacks

Table 1 demonstrated that glacial cycles comprise four or five SGYs, while Table 2 shows that the increased insolation from a Great Summer may be insufficient to cause an interglacial, due to albedo reflections. Which is probably why the Great Summer season 170 kyr ago produced no appreciable warming, despite the 80 W/m^2 increase in NH insolation. Clearly, there must be another factor influencing and modulating interglacial warming periods. Many suggestions have been made to account for this selective response to orbital forcing, including ice-sheet depression of the lithosphere warming the ice sheets (Abe-Ouchi et al., 2013); a brine-induced stratification of the oceans storing CO_2 (Bouttes et al., 2010, 2012); increasing CO_2 concentrations combined with lowering ice-sheet albedo caused by terminal moraine dust (Ganopolski et al., 2010; Ganopolski and Calov, 2011); and a 500 m rise in the Himalaya triggering the post-MPT ice-age era (Kuhle, 1988). Yet the great disparity between these many competing theories highlights the uncertainty that still exists, regarding the true causes of ice-age modulation.

The simple solution is dust. And although dust has been mentioned previously as a feedback agent, notably by Ganopolski, Mahowald and Krinner, it has never been used as a comprehensive solution to the selective orbital cycle problem, and nor have the causes of this dust been fully explored and explained (Mahowald et al., 1999, 2006; Krinner et al., 2006; Ganopolski and Calov, 2011). The IPCC also suggests that dust played a role in paleoclimate feedbacks, but their small allowance for ice albedo reductions is said to be countered by the increased albedo of dust in the atmosphere. The 2007 AR4 report says of this aeolian dust:

> *The effects of atmospheric dust content and vegetation changes give an additional 1 °C to 2 °C of global cooling, although scientific understanding of these effects is very low.* (IPCC AR4 6.4.1.3. See also their Fig. 6.5.)

So the IPCC has identified dust as a net weak cooling mechanism, when it is probably a very strong warming agent. The IPCC's AR4 Fig. 6.5 gives a feedback value of −1.5 W/m^2 for dust during the LGM, due to aeolian dust reducing insolation. This was revised in AR5 to a best estimate of −1.0 W/m^2, while Lambert derived an even larger figure of −3 to −6 W/m^2 (Lambert et al., 2013). But what does not appear to be fully accounted for in these various reports, is the reduction in albedo and the potentially substantial increase in local insolation absorption that this same atmospheric dust can generate when it finally settles upon fresh snow and ice.

Table 2 demonstrated that the difference between Great Winter and Great Summer insolation absorption at 65°N is only about 7 W/m^2, which is not very significant. Which is why the climate continues to cool from the peak temperatures of an interglacial even during clusters of strong Great Summers, because the increased insolation cannot get any leverage on the reflective ice. What a Great Summer requires, in order to be successful and produce a full interglacial, is a layer of dust and

Please cite this article in press as: Ellis, R., Palmer, M., Modulation of ice ages via precession and dust-albedo feedbacks, Geoscience Frontiers (2016), http://dx.doi.org/10.1016/j.gsf.2016.04.004

dirt on the ice-sheets to reduce their albedo. Surprisingly, this is exactly what happened. As can be seen in Fig. 4, every interglacial warming period over the last 800 kyr was preceded by several thousand years of dust storms.

4.2. Albedo reductions by ppm of dust

Fig. 4 demonstrates a close correlation between dust deposition on Antarctic ice sheets and low temperatures during every glacial maximum. The Greenland ice cores show even greater dust deposition before the Holocene interglacial, which demonstrates that these dust eras were global in extent and proportional to proximity with large landmasses. This increase in dust is often thought to be related to a drier glacial climate causing desertification, but a different agent will be invoked shortly. It is significant that peak dust is reached just before temperatures begin to rise during an interglacial, and it is highly likely that this relationship is causal, because the dust is settling on the northern ice sheets and reducing their albedo. But the temperature reaction to dust is not immediate, because the deposition rate is insufficient, and so during this long deposition stage the increasing depth of dust layers is acting as a latent feedback agent. What is required to start the interglacial warming, in addition to dust, is the extra insolation provided by a Great Summer. And as the rapid interglacial temperature increase 130 kyr ago in Fig. 3 demonstrates, as soon as the Great Summer arrives the warming begins.

Levels of dust within Antarctic ice cores are small, averaging just 0.8 ppm at peak dustiness, but the effects of low levels of dust have been demonstrated to be significant. Experiments were carried out in Finland by Svensson and in Siberia by Warren using manmade snow with known quantities of soot impurities, and the albedo response of the snow graphed in Fig. 5a and b was surprisingly large (Warren et al., 2009; Svensson et al., 2015). These graphs show that 1 ppm of soot impurities can reduce albedo from an average 0.90 down to 0.77, while increasing the contaminants to 10 ppm can result in a decrease down to just 0.45 albedo, which are significant reductions. Note that the angle of elevation of the Sun, the size of the snow grains, and any initial contaminants can make a significant difference to the effective albedo of fresh snow, which is why there is a difference between the initial albedo values in these graphs. Svensson and Warren say of their results:

> *A clear effect on albedo and snow melt was visible when soot concentrations of 1 ppm were used, whereas it was more difficult to attribute the soot's effect when lower concentrations of 0.1 ppm were used.* (Svensson et al., 2015)

> *Very small ppm amounts of soil dust in snow can significantly reduce snow albedo and thereby effect the snow surface energy budget.* (Warren et al., 2009)

A reduction from 0.9 to 0.77 albedo on the northern ice sheets would result in a significant increase in insolation absorption across

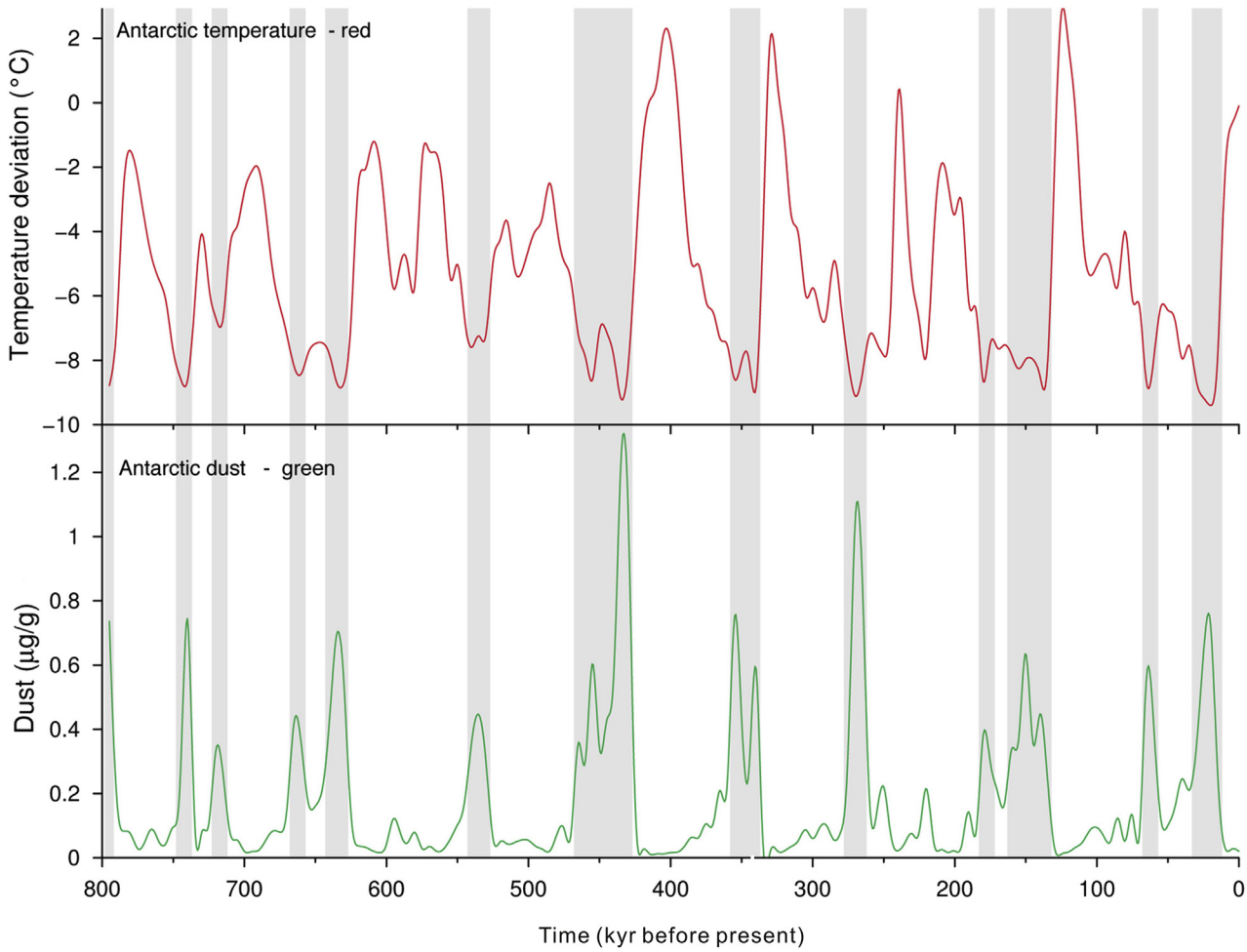

Figure 4. Dust concentrations in ppm vs. temperature for the last 800 kyr, from the Epica3 ice core. Shaded bands highlight dust >0.35 ppm. Note that increased dust deposition occurs just before each interglacial warming. Source: Epica3, 2007.

Please cite this article in press as: Ellis, R., Palmer, M., Modulation of ice ages via precession and dust-albedo feedbacks, Geoscience Frontiers (2016), http://dx.doi.org/10.1016/j.gsf.2016.04.004

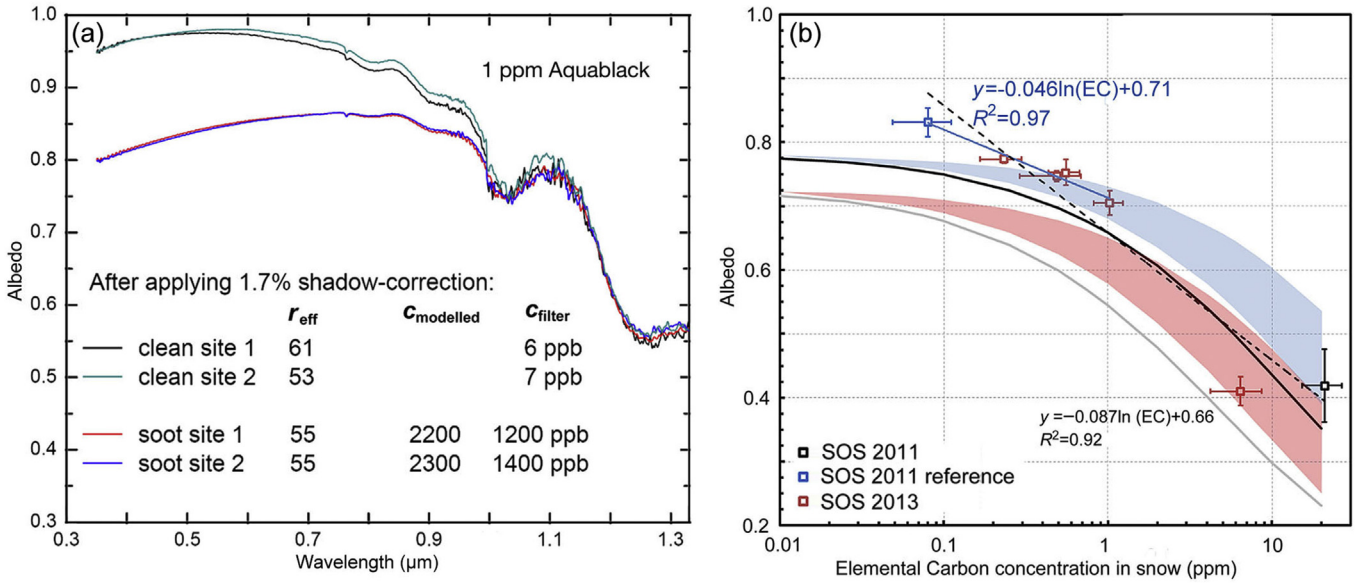

Figure 5. Outdoor albedo testing using manmade snow with known soot contaminant levels. (a) The wavelength of the incoming light is on the x-axis, the visible spectrum being from about 0.4 to 0.7 μm. The difference between clean snow and 1.2 ppm of soot is about 13% (Warren et al., 2009). (b) The blue and red shading represents model simulations, and the data-points are by experimentation. The difference between clean snow and 1.0 ppm soot is about 13% which equates well with Warren's results (Svensson et al., 2015).

the northern hemisphere, while the reduction down to 0.45 allows the ice-sheets to approach the albedo levels of dry sand. However, both these experiments were conducted with soot particles and Warren reports that soot is 50× more effective than dust at generating albedo reductions. But this reduction in dust effectiveness is countered by Greenland receiving up to 10× the dust concentrations of Antarctica (8.0 ppm at Ngrip vs. 0.8 ppm at Epica3) (Ruth et al., 2007). And we might also speculate that the levels of dust deposited at the lower latitudes of the Laurentide and Asian ice sheets, closer to the sources of the dust, might contain 3× more dust than the samples in the Ngrip ice core which is located at 75°N. This is a conservative estimate as Mahowald's model simulations indicated ten times more dust deposition over the Laurentide ice sheet near the Great Lakes, than on central Greenland during the LGM (Mahowald, 1999; plate 5b). In which case, the total dust contamination on the southern portions of the northern ice sheets might be about 25 ppm, and have an effective soot-equivalence of 0.5 ppm, and so the equivalent albedo would reduce from 0.90 to about 0.85.

4.3. Concentration of surface dust

While a 6% drop in albedo is insufficient to cause an immediate warming of the northern ice sheets and a global temperature response, as Fig. 4 clearly demonstrates, a limited regional warming event would increase the concentration of surface dust considerably as each year-layer of ice was melted or ablated. Warren confirmed in his paper that: '*impurities tend to collect on the surface rather than washing away with the meltwater*' (Warren, 1984). Eroding just ten year-layers of snow and ice could increase surface dust concentrations by an order of magnitude, and so the dust would continue to thicken over the years as more dust-laden ice was melted or ablated, until the surface of the northern ice sheets looked something like the glacial ice in Fig. 6a and b. Both of these images confirm that dust and impurities collect on the surface of glaciers.

It is likely that a considerable thickness of the northern ice sheets would have been contaminated by these millennial dust storms. At the Gisp2 ice core in central southern Greenland at 72°N

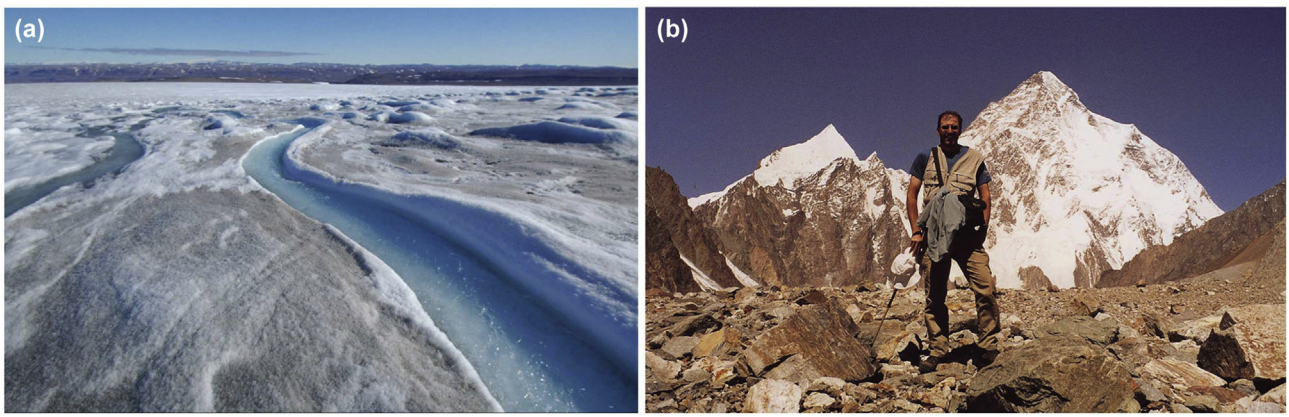

Figure 6. (a) A region of ablated glacial ice on the Greenland ice sheet, demonstrating that annual contaminants can concentrate on the surface, rather than getting washed away. Photo: Stephen Warren. (b) The author standing on the very center Baltoro Glacier in the Himalayas. Surface ice quickly melts, because the albedo-assisted daytime temperatures are quite high, even in October at 5500 m altitude, leaving a rocky ice-free surface.

Please cite this article in press as: Ellis, R., Palmer, M., Modulation of ice ages via precession and dust-albedo feedbacks, Geoscience Frontiers (2016), http://dx.doi.org/10.1016/j.gsf.2016.04.004

the dateable ice sheet is 2800 m thick, representing 110 kyr of ice layers (plus another 250 m of undatable ice). But the upper 1560 m of this represents just 10 kyr of ice deposition (Taylor et al., 1997). If the Holocene had experienced a 10 kyr dust storm era, then the upper 55% of the ice sheet would contain dust contaminants. However, the deposition and flow dynamics of the ice sheets were quite different during the LGM. Snow accumulation was only 6 cm/yr rather than the 24 cm/yr deposited during the Holocene, which might initially suggest that the ice sheet over Greenland was thinner at the LGM (Cuffey and Clow, 1997). At Gisp2 the modern deposition rate is 50 cm p.a. (Taylor et al., 1997). But the lower LGM accumulation rate was balanced by a much greater ice sheet extent, which buttressed the Greenland ice-dome and reduced basal outflow and thinning. Thus Cuffey determined that there was probably not much change in the thickness of the ice sheet at Gisp2 in central Greenland, in comparison to its present 3050 m (Cuffey and Clow, 1997). When combined with reduced accumulation rates, reduced outwards flow, and reduced basal thinning during the glacial maximum, this great thickness would mean that the age profile of the ice sheet was not as steep as it is today. So while the most recent 10 kyr of ice currently occupies the top 55% of the ice sheet at Gisp2, during the glacial maximum it may have only occupied the top 25%. Even so, this would still mean that the 15 kyr of dust storms experienced just before the interglacial may have contaminated the upper third of the northern ice sheets.

It is unlikely that albedo melting would have taken place on the upper plateau of the Laurentide and Asian ice sheets, because they reached 3000 m in altitude and were 20 °C colder than at sea-level (Dyke et al., 2010). And we can be confident that melting did not occur over central Greenland because the LGM ice-layers are still extant. But the lower-level ice sheet terminations would have been highly susceptible to warming, especially where they sloped towards the south. And once albedo melting and ablation had begun, dust concentration would intensify the albedo feedback very rapidly and the warming and melting would be difficult to stop. As long as there were still dust-laden layers of ice to melt, dust would continue to concentrate on the surface and the albedo would continue to decrease. However, there is a limit to these insolation absorption increases, which is reached when the thickness of the dust layer reaches about 7 mm, at which point the dust starts to act as an insulator rather than an albedo-reducing warming feedback. However, Warren calculated that even with 10× the dust concentration found in the Greenland ice cores, it would take 2000 m of ice-melt to reach this level of surface dust, and so this is not a limitation (Warren, 1984).

There is one other consideration to take into account during the dusty glacial maximum era and that is the negative forcing of dust in the atmosphere, as discussed in Section 4.1. The peak insolation reduction for atmospheric dust from Lambert was about −5 W/m^2. However, since the glacial maximum was much colder and drier in the polar regions, cloud albedo would also have reduced at this time. And since the value of glacial cloud albedo has not been adequately established, we might simply presume that the increase in atmospheric dust albedo was balanced by a decrease in atmospheric cloud albedo. In which case, the total atmospheric insolation reductions remain at −20%, as previously calculated, and while this assumption may seem arbitrary there is insufficient data to make a more accurate estimate. Taking into account these many considerations, the increases in annual regional midsummer insolation and absorption for dust-contaminated ice-sheets are given in Table 3.

Table 3
Difference in insolation and absorption for dusty ice vs. clean ice (based upon Table 2).

Great Winter (annual midsummer)	
Ice sheet insolation (less cloud & haze)	360 W/m^2
Fresh ice absorption at 0.90 albedo	36 W/m^2
Dusty ice absorption at 0.85 albedo	54 W/m^2
Increased absorption due 20 ppm dust	18 W/m^2
Great Summer (annual midsummer)	
Ice sheet insolation (less cloud & haze)	430 W/m^2
Fresh ice absorption at 0.90 albedo	43 W/m^2
Dusty ice absorption at 0.85 albedo	65 W/m^2
Increased absorption due 20 ppm dust	30 W/m^{2*3}
Dusty ice absorption due 200 ppm dust	170 W/m^2 (0.60 albedo)
Increased absorption due 200 ppm dust	135 W/m^{2*3}
Dusty ice absorption due 400 ppm dust	215 W/m^2 (0.50 albedo)
Increased absorption due 400 ppm dust	180 W/m^{2*3}

55°N ice sheet dust assumed as NGrip 8 ppm × 3 = 24 ppm.
25 ppm dust = 0.5 ppm soot equivalent, 200 ppm dust = 4.0 ppm soot equivalent. From Svensson, soot and albedos are: 0.5 ppm = 0.85, 4.0 ppm = 0.60, 8.0 ppm = 0.50.
Just 10 year-layers of ice ablation required to increase from 25 ppm to 200 ppm of dust.
*3 Compared with the Great Winter 0.90 albedo absorption.

4.4. Causes of glacial-maximum dust

It has been suggested that these sudden dust eras at each glacial maximum were caused by the ice sheet termini encountering silt deposits further south during successive glaciations (Ganopolski et al., 2010; Ganopolski and Calov, 2011). But this scenario is not supported by the geology, as the Sand River region of Saskatchewan in Canada still bears 50–80 m of sediments that predate the last Wisconsin glaciation, and the Lower Empress sediment formation predates the entire Pleistocene epoch (Fenton et al., 1994). So the geological evidence indicates that glaciation does not remove the underlying alluvial deposits in the manner described. Alternatively it has been claimed that a cooler atmosphere cannot hold as much moisture, resulting in widespread desertification (Petit et al., 1999, p5). The aridity theory is supported by the polar ice accumulation record, which shows less snow deposition and presumably a much drier climate during the depths of the ice-age (Allen, 2000). And while this may have been true for the polar regions, where temperatures dropped dramatically, the situation in the tropics was quite different.

Modern average tropical temperatures, taken from 12 random locations close to the equator, range from an average low of 24.7 °C to an average high of 27.6 °C (Climate Temperatures, 2014). The temperature difference between modern and glacial conditions in the tropics has not been precisely established, for reasons that will become apparent shortly. The IPCC AR4 report gives an average drop in temperature of −2 to −3 °C across most of the tropics, while IPCC AR5 5.3.2.2 gives global temperature reductions ranging from −1.7 to −8.3 °C. But the polar regions were much colder, which skews these global temperature reductions towards the lower range. A better data source is the Paleoclimate Modeling Intercomparison Project (PMIP3), which provides an average of eleven LGM temperature models from established climate modeling agencies (PMIP3, 2015). The result in Fig. 7a shows a broad band of glacial temperatures that are about 3.5 °C lower than present values.

This modest temperature reduction would result in average tropical temperatures of 21 to 24 °C, which are quite high enough to produce oceanic evaporation and therefore generate tropical and extratropical rainfall. So although there were changes in precipitation patterns during the glacial maximum, the world was far from becoming a barren and dusty desert due to a lack of precipitation. Confirmation can be seen in the PMIP3 precipitation map in Fig. 7b, which is derived from eleven established glacial maximum models. This shows a band of lower rainfall across the tropics of the Americas and Africa, which widens out across southeast Asia and

Please cite this article in press as: Ellis, R., Palmer, M., Modulation of ice ages via precession and dust-albedo feedbacks, Geoscience Frontiers (2016), http://dx.doi.org/10.1016/j.gsf.2016.04.004

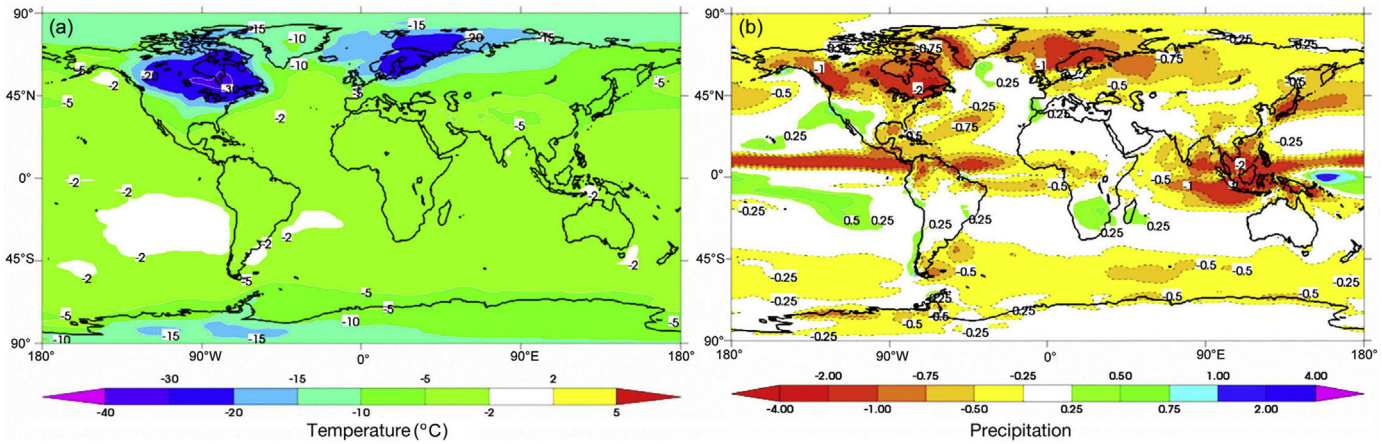

Figure 7. (a) LGM to modern temperature comparison. The large band across the tropics and beyond shows an average −3.5 °C temperature reduction. Source: PMIP3. (b) LGM to modern precipitation comparison. Apart from ice sheet regions, rainfall reductions are limited to select tropical regions. Source: PMIP3.

Indonesia. However, most other regions including the region around northwestern China and Mongolia retain similar or slightly increased precipitation levels to the present climate, and this will become significant later (PMIP3, 2015). As these two charts demonstrate, the glacial maximum world was far from becoming a cold and barren desert due to either precipitation or temperature reductions. So if there was a large extension of desert regions that generated these global dust storms, there may well be another environmental factor that has not been fully accounted for.

5. Flora, CO_2 and dust generation

5.1. Effects of low CO_2 on flora

The additional factor involved in glacial maximum desertification and dust production is likely to be low concentrations of CO_2. Fig. 8 demonstrates that high dust concentrations are not only linked with low temperatures, they are also closely linked to low CO_2 concentrations. But the reason for the CO_2 reduction and its possible connection to the increase in dust is poorly understood. The 2007 IPCC AR4 report said:

> *The quantitative and mechanistic explanation of these CO_2 variations remains one of the major unsolved questions in climate research.* (IPCC AR4 Box 6.2. What Caused Low Atmospheric CO_2)

Once again the science appears to be wanting. Several mechanisms for CO_2 sequestration were suggested in this IPCC report, including calcium carbonate weathering, coral reef growth, and dust-fertilisation and sedimentation of marine organisms. But these are all very slow processes, and therefore struggle to explain how the sequestrated CO_2 returns 100 ppm back to the atmosphere within a short 5 kyr of interglacial warming.

A more logical explanation for the inverse correlation between dust and CO_2 can be seen through the effect that CO_2 concentrations have on plant life. Fig. 8 also shows that CO_2 levels during each ice-age came all the way down to 190–180 ppm, and that is approaching dangerously low levels for C_3 photosynthesis-pathway plant life. CO_2 is a vital component of the atmosphere because it is an essential plant food, and without CO_2 all plants die. In her comprehensive analysis of plant responses to reduced CO_2 concentrations, Gerhart says of this fundamental issue:

> *It is clear that modern C_3 plant genotypes grown at low CO_2 (180–200 ppm) exhibit severe reductions in photosynthesis, survival, growth, and reproduction … Such findings beg the question of how glacial plants survived during low CO_2 periods … Studies have shown that the average biomass production of modern C_3 plants is reduced by approximately 50% when grown at low (180–220 ppm) CO_2, when other conditions are optimal … (The abortion of all flower buds) suggested that 150 ppm CO_2 may be near the threshold for successful completion of the life cycle in some C_3 species.* (Gerhart and Ward, 2010 Section II)

It is clear that a number of plant species would have been under considerable stress when world CO_2 concentrations reduced to 200 or 190 ppm during the glacial maximum, especially if moisture levels in those regions were low (Gerhart and Ward, 2010; Pinto et al., 2014). And palaeontological discoveries at the La Brea tar pits in southern California have confirmed this, where oxygen and carbon isotopic analysis of preserved *juniperus* wood dating from 50 kyr ago through to the Holocene interglacial has shown that: '*glacial trees were undergoing carbon starvation*' (Ward et al., 2005). And yet these stresses and biomass reductions do not appear to become lethal until CO_2 concentrations reach 150 ppm, which the glacial maximums did not achieve - unless we add altitude and reducing CO_2 partial pressures into the equation.

The suggestion that altitude could be a factor was countered by Terashima, who asserted that CO_2 partial pressure reductions with altitude would only have a small effect on photosynthesis, because the lower CO_2 partial pressure is partly compensated by increased diffusion of gases at lower atmospheric pressure (Terashima and Yokoi, 1995; Johnson et al., 2005). However, this increased gaseous diffusion will not influence the transport of CO_2 through the aqueous phase of the chloroplast, which limits this effect (Shi et al., 2015). In addition, lower partial pressures also increase transpiration, which when combined with greater insolation and a drier atmosphere at high altitude, increases stomatal moisture loss considerably. Another limiting factor is the standard plant response to reducing atmospheric CO_2 concentrations, which is to increase stomatal numbers or area to increase gas diffusion, but this again increases transpiration and water loss (McElwain, 2004; Johnson et al., 2005; Shi et al., 2015). So reducing partial pressures of CO_2 could well limit plant growth with altitude, especially in moisture deficient regions where the effects of CO_2 reductions are enhanced via a moisture proxy.

Shi also conducted real-world experimentation on high altitude photosynthesis and growth, and found that while some species displayed a range of strategies to combat reducing CO_2 partial pressure with altitude, other species like the *Quercus spinosa*

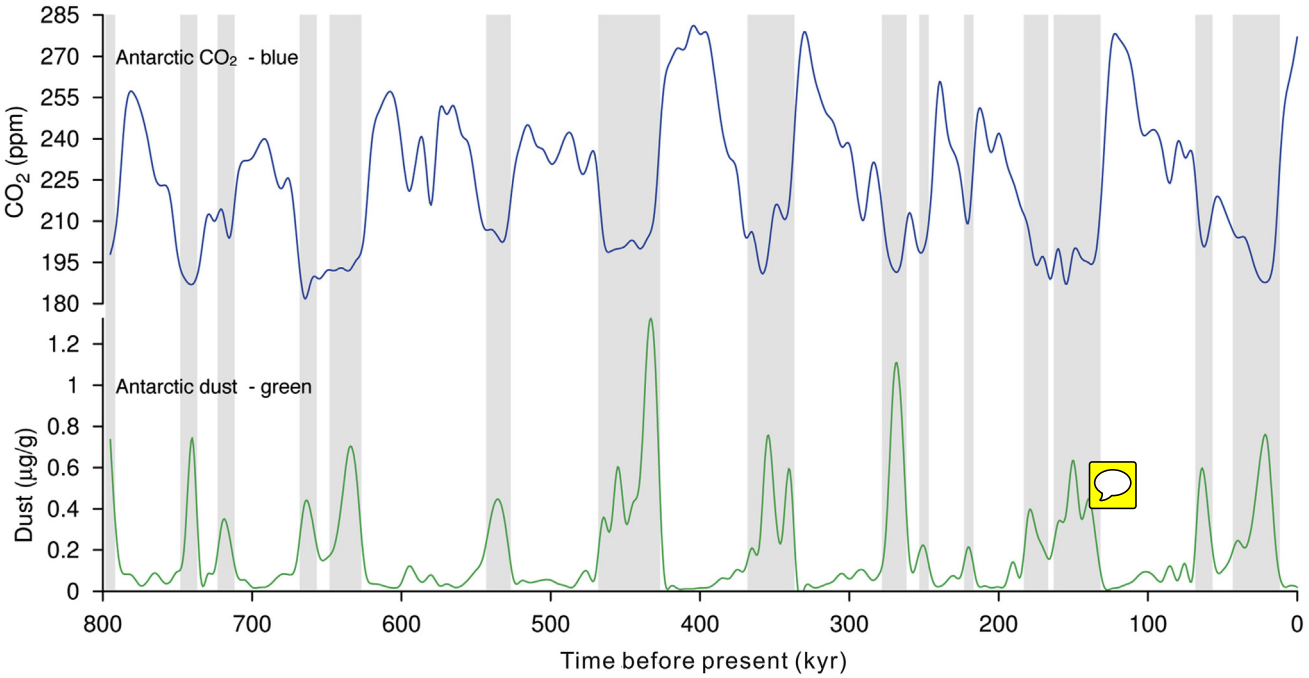

Figure 8. Dust deposition vs. CO_2 concentrations in ppm. Note that low CO_2 concentrations always result in high dust concentrations. It is likely that CO_2 concentrations are the causal factor here. Source: Epica3, 2007.

evergreen oak tree barely responded at all, and showed markedly reduced photosynthesis with increasing altitude. Further experimentation was performed on individual leaves, measuring the photosynthesis response to a variety of CO_2 concentrations at two different partial pressures (2500 m and 3500 m). This demonstrated that even in species that responded positively to counter low CO_2 partial pressures, photosynthesis efficiency reduced steeply below 200 ppm CO_2, at both of the partial pressures tested (Shi et al., 2015). And the plants in these experiments were not subject to the added complication of moisture stress.

Contrary to Terashima's model of plant responses to CO_2 partial pressures, real-world experimentation paints a more complex picture. Photosynthesis efficiency reduces steeply below 200 ppm CO_2, at all partial pressures (all altitudes), while the increasing moisture demands associated with reducing CO_2 partial pressure will significantly reduce photosynthesis and survivability. When combined, these two factors will ensure that increasing altitudes will significantly inhibit plant growth and survivability, especially in regions that are moisture deficient. While lesser adapted trees like the *Q. spinosa* evergreen oak will be limited by reducing CO_2 partial pressures (increasing altitudes) whatever the moisture levels. Shi suggested that the lack of CO_2 adaption by *Q. spinosa* was due to its evergreen nature, which requires maintaining stomatal changes during winters or dry seasons when such adaptions may be detrimental, and so this lack of adaption may pertain to other evergreen species.

5.2. C_3 and C_4 flora differences

The studies by Terashima, Gerhart and Shi focus on C_3 plants, which have a less efficient system of photosynthesis for fixing CO_2 than C_4 plants. C_4 plants are a recent evolutionary adaptation that utilize a two-step photosynthesis process, which has the effect of concentrating CO_2 before the final fixation step. However, despite the greater CO_2 fixation efficiency of C_4 plants, some 85% of the worlds plant species remain in the C_3 category, and these include many of the world's cereal crops like wheat and barley; half of the grasses; and all of the woody trees (Moore et al., 1995). And some 95% of the world's biomass is still comprised of C_3 flora (Still et al., 2003; Körner et al., 2010).

In comparison, only 3% of plant species are C_4, but these comprise the highly successful cereal crops like maize and sugarcane; half the grasses; and many sedges (Moore et al., 1995). C_4 plants are said to make up 23% of the present annual plant CO_2 fixation, although this remarkably high figure is strongly biased towards C_4 plants by modern agriculture, which has decimated great swathes of ancient C_3 forests and replaced them with C_4 sugarcane and maize (Still et al., 2003; Osborne and Beerling, 2005). There was also a bias towards C_4 plants at high altitude during the LGM, as will be discussed later, because these two types of plant display significant differences in their response to environmental factors. These differences include:

(1) C_3 plants become more efficient than C_4 plants at low temperatures (giving C_3 plants a competitive advantage in cool conditions);
(2) C_3 plants are much less tolerant of low CO_2 conditions (low CO_2 concentrations below 180 ppm will adversely effect C_3 species);
(3) C_3 plants need more moisture in low CO_2 conditions (a dry climate with reducing CO_2 concentrations will adversely effect C_3 species).

5.3. Effects of low CO_2 on treelines

The modern mountain treeline varies from 2000 m in the Alps to 4000 m in the tropics, and is temperature rather than CO_2 limited (Körner and Paulsen, 2004). But the balance and interplay between these upland C_3 forests and savannahs and the (generally) lower level C_4 regions would change dramatically during the reduced CO_2 conditions of a glacial maximum, with upland C_3 forests and savannahs suffering the greatest stress. Table 4 shows the reduction in temperatures and CO_2 partial pressure concentrations for a range

Please cite this article in press as: Ellis, R., Palmer, M., Modulation of ice ages via precession and dust-albedo feedbacks, Geoscience Frontiers (2016), http://dx.doi.org/10.1016/j.gsf.2016.04.004

of regions and altitudes. The critical treeline temperature is defined by a minimum average root temperature of 6.5 °C (Körner and Paulsen, 2004), while the critical average air temperature can be much lower. The critical CO_2 extinction-concentration is assumed to be between 160 and 150 ppm equivalent (160–150 μbar) (Gerhart and Ward, 2010). The limiting factor for glacial and interglacial treelines in Table 4, is underlined in each case.

If the critical sea-level CO_2 concentration for C_3 trees and grasses is between 160 and 150 ppm, Table 4 demonstrates that the modern interglacial treeline is limited by temperature rather than CO_2. But during glacial maximum conditions, when tropical sea-level temperatures fell by 3.5 °C and sea-level CO_2 concentrations reduced to 190 ppm, CO_2 definitely becomes the primary limiting factor for high altitude C_3 forests and savannahs, especially in tropical regions. Depending on the response of individual species to CO_2 deprivation, Table 4 suggests that the tropical treeline may have reduced from 4000 to 1700 m, equating to an equivalent CO_2 concentration of 150–160 ppm (150–160 μbar). Field studies have demonstrated this effect, but have interpreted the treeline reductions as implying large decreases in temperature, as will be discussed shortly. Snowlines would also have reduced, covering some of this newly exposed land, but Porter suggests a reduction in tropical regions averaging 750 m at the LGM (Porter, 2000). The difference between these two factors is about 1500 m, and since land area increases exponentially with reducing altitude this ensures that large expanses of newly barren land would have been created by glacial CO_2 reductions.

This theoretical calculation for the CO_2 regulation of glacial maximum treelines appears to be confirmed by Behling's study of peat bogs on the Campos do Jordao plateau near Sao Paulo in Brazil, which lies at 1850 m amsl. The cores found grey sand deposits almost devoid of organic material during the LGM period, overlain by thick peat deposits all through the Holocene. Similarly, the pollen grain record of the Holocene peats revealed a thickly forested region, while the LGM grey sands showed that these interglacial forests: '*did not exist in the study area during the late Quaternary period*' (ie: during the LGM). In their place were pollen grains from 'high elevation grasslands', but these could not have been lush pastures as the grey sands showed '*little in the way of organic material*' (Behling, 1997).

Behling also observed that araucaria forests and plantago grasses, which enjoy cool-moist and cool-dry conditions respectively, were missing from the grey sands. So Behling was forced to conclude that there was a much colder and possibly dryer climate on the Campos do Jordao plateau during the LGM, with a reduction in temperature of 5–7 °C, even though this conflicted with other climate studies in this region (Behling, 1997). A possible reason for this discrepancy is CO_2. The Campos do Jordao lies at 1850 m altitude, which is coincident with the tropical CO_2 treeline altitude suggested in Table 4. So the Campos do Jordao region may well have been warmer than claimed during the LGM, but could still not support C_3 forests and grasslands at that low CO_2 partial pressure altitude.

Willie performed a similar analysis of treelines on and above the 1800 m Popayán plain in Columbia. The upper treeline in this region had reduced from its present 3500 m, to 2000 m during the LGM, which was attributed to lower glacial temperatures (Willie et al., 2000, 2001). Although Bakker reports a pollen-free clay layer at the LGM, which would suggest a treeline at 1700 m or below during the LGM and would agree with the results in Behling's study (Bakker et al., 1990). CO_2 concentrations were mentioned in Willie's study, but thought not to be significant for altitudes below 2500 m because: '*the impact of low atmospheric CO_2 on temperature reconstructions is not available, and the debate quantifying its impact is still ongoing*'. But the rejection of CO_2 treeline regulation necessitated a LGM temperature reduction of 6 – 7 °C at 1700 m, while Bakker derived an even larger fall of 8–10 °C (Bakker et al., 1990).

These large temperature reductions gave researchers a problem, because the 1981 CLIMAP study had determined from sediment and fossil analysis that sea temperatures around Columbia were only 2 °C cooler during the LGM, while sea-level land temperatures were only 2.5 °C cooler (Rind and Peteet, 1985, p11; Climap, 1981). This small temperature change conflicted greatly with the 6 – 10 °C fall in temperature indicated by treeline and species variation up in the Popayán highlands. The first resolution to this problem was to arbitrarily lower the sea level temperatures by 2 °C in the CLIMAP model, which reduced the differential between sea-level and highland temperatures (Rind and Peteet, 1985). Although the temperature reduction at 2500 m on this revised model run was still only 3 °C, instead of the 6 – 10 °C reductions being reported in the field. But these large temperature reductions resulted in a significant increase in the region's environmental lapse rate from its present 6 °C/1000 m to 7.6 °C/1000 m at the LGM, which in turn suggested a large and widespread reduction in humidity and precipitation across this region. Yet this conflicted with lower level recolonisation during the LGM by tree species that favoured moist conditions (Willie et al., 2000, 2001).

Although they became widely accepted, these high lapse rates and corresponding regional aridity are meteorologically anomalous. Even back in 1984 they were being called into question, with Rind saying of the Columbian lapse rate issue:

> *A large divergence in lapse rate from the moist adiabatic value is implausible, as moist convection should still represent the dominant vertical heat transportation process at low altitudes. Webster and Streten (1978) concured, and showed that at low latitudes even arid stations have lapse rates close to moist adiabatic* (Rind and Peteet, 1985).

This was confirmed in an analysis of modern lapse rates in Arizona, which demonstrated a mean terrain-following lapse around Tucson of just 5.7 °C/1000 m ± 0.6 °C, and it is the terrain-following

Table 4
Reductions in temperature and CO_2 affecting the maximum treeline in the Alps and tropics.

Factor limiting the C_3 treeline	Alpine treeline				Tropical treeline					Tropical Snowline
	Surface	1000 m	1500 m	2000 m	Surface	1000 m	1500 m	2000 m	4000 m	
Interglacial temps (°C)	15	9	6	3	28	22	19	16	4	~4800
Interglacial CO_2 (μbar)	300	265	250	235	300	265	250	235	180	
Glacial temps (°C)	11	5	3	−1	24	18	15	12	−0	~3950
Glacial CO_2 (μbar)	190	170	160	150	190	170	160	150	115	

The limiting factor for the treeline is underlined in each case.
Tropical adiabatic lapse rate 6.0 °C/1000 m. Standard SL pressure 1013.25 mb.
ICAO pressure altitudes 1000 m = 900 mb, 1500 m = 845 mb, 2000 m = 795 mb, 4000 m = 615 mb.
300 ppm sea-level CO_2 concentration assumed, to show the historic situation.
Snowlines from Porter, average of 10 sites. There is great data variability (Porter, 2000 Table 1).

Please cite this article in press as: Ellis, R., Palmer, M., Modulation of ice ages via precession and dust-albedo feedbacks, Geoscience Frontiers (2016), http://dx.doi.org/10.1016/j.gsf.2016.04.004

lapse rate that hillside vegetation will be experiencing and reacting to (Harlow et al., 2004). So even in the arid conditions of Arizona, the average hillside lapse rate is equivalent to the modern Columbian lapse rate of 6.0 °C/1000 m, and significantly less than the assumed Columbian LGM lapse rate of 7.6 °C/1000 m. This was supported by an analysis of preserved LGM *juniperus* wood from the La Brea tar-pits in southern California, which demonstrated a 10% increase in relative humidity during the LGM in comparison to Holocene values (Ward et al., 2005). And although California and Columbia are separated by some 5000 km, this does demonstrate that the LGM climate was not universally arid. However, since the assumed high LGM lapse rate in Columbia pointed towards greater aridity in that region, this conjecture appears to have been incorporated into the PMIP precipitation map in Fig. 7b which has a localised area of low precipitation centered on Columbia. So these treeline 'temperature gauges' appear to have modified climate model results ever since the 1980s. But if the true cause of these high altitude treeline and species changes was CO_2 concentrations, then these temperature, lapse rate and moisture adjustments are unwarranted, and the PMIP model may be displaying erroneous results.

Hooghiemstra's similar survey in the same region observed that the LGM paramo grasslands and scrublands may have extended up to 3200 m during the LGM, which is substantially higher than the calculated CO_2 extinction altitude in Table 4. But this was primarily due to a recolonisation of these regions by C_4 plants (Hooghiemstra and Van der Hammen, 2004), presumably because C_4 plants are more tolerant of low CO_2 conditions. However, since C_4 plants are not so tolerant of cold conditions, this again suggests that large reductions in temperature were not the primary factor determining LGM treelines above the Popayán plain.

Several models have been devised to replicate and explain the treeline data gathered here, and many now include the effects of low CO_2 on vegetation. In 1997 Jolly ran an early BIOME4 vegetation model coupled with the IIASA climate database, and demonstrated that when temperature was the primary controlling factor a 6.5 °C reduction was required to reproduce LGM treelines, and yet no temperature reductions were required if CO_2 was reduced to 190 ppm (Jolly and Haxeltine, 1997). So this modification would eliminate the anomalously high lapse rates that plagued the Columbian research. Jolly went on to say that this CO_2 effect was not caused by partial pressure reductions with altitude, because of the diffusion compensation effect explained previously, and so the influences of CO_2 reductions on plant survival are to be expected at all altitudes. But this assertion conflicts with the model results, which demonstrated a clear relationship between treelines and altitude even when precipitation remained the same. This dichotomy was not explained. A decade later Wu investigated the upgraded BIOME4 vegetation model coupled with the MARGO ocean circulation model and pollen-based treeline records from across Africa. The results again demonstrated that anomalously high lapse rates could be eliminated if CO_2 concentrations were reduced to LGM levels (Wu et al., 2007). If these model simulations are correct, then the primary factor controlling treelines and highland vegetation survival must be CO_2, rather than temperature.

A more comprehensive study was undertaken by Woillez, using the ORCHIDEE vegetation model coupled with the IPSL-CM4 atmosphere circulation model. The results again demonstrated that low CO_2 may well have been the most significant factor in the regression of forest treelines during the LGM. Woillez says of this:

> *(The) Last Glacial Maximum reveals landscapes radically different from modern ones, with a massive regression of forested areas in both hemispheres … Our modeling results support the view that the physiological effect of glacial CO_2 is a key factor to explain vegetation changes during glacial times. In our simulations, the low atmospheric CO_2 is the only driver of the tropical forest regression, and explains half of the response of temperate and boreal forests to glacial conditions* (Woillez et al., 2011).

A more recent model reconstruction was reported by Claussen, using the JSBACH vegetation model coupled with the ECHAM6 atmosphere circulation model. This confirmed the work of Woillez but did not see any recovery of deforested regions by grasses, possibly because Claussen's model accounted for partial pressures with altitude (Claussen et al., 2012). Neither Woillez nor Claussen's papers mention CO_2 partial pressures, but it was confirmed in private correspondence that the latter model does take this factor into account, although to what degree is unknown. Claussen's simulations demonstrated a three-fold decrease in vegetation during the glacial maximum, when CO_2 reductions were included. This represents a 26×10^6 km^2 increase in barren areas, which amounted to about 20% of the glacial world's habitable land surface at that time. This represents a considerable increase in newly exposed and dusty regions, much of which would have been in upland locations. Claussen says of this:

> *The pure ecophysiological effect of CO_2 appears to be stronger than the pure climate effect for many plant functional types … In line with previous simulations, the MPI-ESM (model) yields a decrease in areas of … extratropical trees by some 45%. The area covered by grassland decreases by some 40% … The desert area increases by 36%* (Claussen et al., 2012).

While temperature-based vegetation models result in implausible temperatures, aridity and lapse rates, these CO_2-based simulations give more reasonable results in all situations. In which case, low CO_2 concentrations are likely to have been responsible for a massive retreat of forests and grasslands, and the first regions to suffer would have been those located in:

(1) High altitude regions, where CO_2 partial pressures would be less than at sea level.
(2) Arid regions, because C_3 trees require more moisture when CO_2 concentrations are low.
(3) Northern regions during July to September, when CO_2 levels reduce (OCO-2, 2015).

5.4. CO_2 and dust creation

If CO_2 reductions during the cooling period of a glacial cycle are capable of causing a global dieback of high altitude flora, this could explain the large increase in dust levels at the end of each glacial maximum. Fig. 8 demonstrates that the initial 60 ppm fall in CO_2 during the glacial cooling period did not significantly affect dust levels; it was only when sea-level concentrations reached a critical threshold, which the shaded bands suggest is about 190–200 ppm, that there was a significant dust-response. And this was not simply a response to falling temperatures, because the many vegetation models demonstrate that the majority of the decrease in upland forests and grasslands was due to CO_2 reductions. And tropical forests actually responded positively to lower glacial temperatures, and only reversed once CO_2 had reduced to the critical threshold. Yet despite the obvious connection between CO_2 and plant survival, the majority of papers do not link CO_2 and dust production. One exception is Mahowald who, while not factoring in altitude or partial pressures, says of CO_2 and dust production:

> *There is little doubt that CO_2 concentrations at LGM levels of 200 ppm would be severely limiting to the productivity of ecosystems, especially in water-limited environments. In a separate sensitivity experiment, roughly half the simulated increase in dust loading was found to be due to the change in CO_2. This result*

suggests a previously neglected indirect role for atmosphere CO_2 in modulating the dustiness of the global atmosphere (Mahowald, 1999).

The close correlation between CO_2 and dust levels can be seen in Fig. 9, which plots CO_2 vs. Antarctic dust, with the dust plot inverted and to a logarithmic scale to reduce the amplitude peaks. On this revised scale CO_2 and dust are very closely inversely correlated, with lower CO_2 levels precisely matching (and potentially causing) the variation in dust. This graph also demonstrates that small changes of CO_2 at relatively high 240–260 ppm concentrations can still cause a slight dust response, even though concentrations above 200 ppm should not be critical to flora in normal conditions. The likely reason is that these higher CO_2 concentrations can still have an effect on C_3 plants at high altitude. A 10 ppm fall in sea-level CO_2 concentrations can lower the high altitude CO_2 extinction-zone and treeline by approximately 300 m, while the equivalent temperature-zone reduction in the tropics would only be 0.35 °C or 60 m. Which again demonstrates that CO_2 is the primary limiting factor. So with each reduction in global CO_2 more land at increasingly lower levels will be denuded of plant-life, creating barren uplands and increasing amounts of dust. And these new desert regions will not be the familiar moisture depletions deserts, but a new breed of upland CO_2 depletion deserts.

But where did the dust preserved in Arctic and Antarctic records come from? Antarctic dust has been positively identified by its unique mineralogy, geochemistry, and isotopy as originating from Argentina (Muhs et al., 2014; Vallelonga and Svensson, 2014). It was initially thought that the dust source might be the newly exposed continental shelf (see also Fischer et al., 2007), but further research determined that the source was more likely to be central Patagonia (Delmonte et al., 2004; Vallelonga and Svensson, 2014). Interestingly, there was a slight difference in the isotopic ratios between glacial and interglacial dust deposits, indicating a slight shift in the source region (Vallelonga and Svensson, 2014).

In contrast, Greenland dust deposits have consistently pointed towards an Asian source around northern China, and this has been narrowed down in more recent research to the Taklamakan and Gobi deserts (Bory, 2014; Vallelonga and Svensson, 2014). Not all desert regions produce dust, because the source region has to contain unconsolidated glacial, alluvial or aeolian loess with an appropriate grain size, and be subject to sufficient wind-strengths (Muhs et al., 2014). Surprisingly, the Gobi Desert is not the primary dust source for modern Greenland dust, because much of the Gobi is pastural steppeland, while the Taklamakan lies in the föhn-wind rain-shadow of the Himalaya and is a true shifting-sand desert. And the presence of these perennial dust-deserts may be why Alaska never had an ice sheet, despite its northerly location and its isolation from the warm waters of the Pacific by the Bearing Straits land bridge. It has been claimed that the lack of Alaskan ice was due to aridity (Elias and Brigham-Grette, 2013), but it is also possible that the region experienced greatly increased dust contamination, which prevented ice accumulation through albedo reductions. Significant aeolian sand deposits have been documented along the Yukon coastline, which remained ice free during the last glaciation, indicating strong aeolian dust activity in the region (Bateman and Murton, 2006). The model simulation by Krinner suggested that this is a likely scenario (Krinner et al., 2006).

The isotopic fingerprint of LGM dust in Greenland is slightly different to modern dust, which again indicates a slight shift in the location of the primary dust-source (Bory, 2014). The usual reason given for this geographic shift is that the climate at the LGM was colder and drier, which could have extended the range of the Gobi Desert. But as was mentioned in Section 4.4, the PMIP LGM precipitation map in Fig. 7b indicates that although some regions of southern and eastern China experienced reduced rainfall, the majority of the Gobi region received the same rainfall during the LGM as in the Holocene interglacial. In fact, Yu and McGee reported that several lakes or lake beds throughout the Gobi region had much higher water levels during the LGM than in the Holocene (Yu et al., 2003; McGee et al., 2010). And despite the modern Gobi being classified as a desert, the majority of the region is still not a shifting-sand desert. Because the winter is long and very cold, and the limited precipitation falls during the short summer, much of the region is steppe grassland. For instance, the town of Dalanzadgad lies within the Gobi Desert region and only receives an average of 130 mm of rain a year (NOAA NCDC). But because this precipitation is coincident with the short summer growing season the land manages to support good pasture for a variety of ruminants, as can be seen in the pastoral map in Fig. 10.

Besides aridity, the other climatic component that may explain the increase in Asiatic dust during the LGM is wind. However, the dust grain size data in both Antarctica and Greenland suggest that winds did not change a great deal between glacial and interglacial climates. In Antarctica Fisher compared dust deposition rates at the EDC and EDML drill sites, which are situated on opposite sides of Antarctica, and demonstrated that: '*parameters for dust transport*

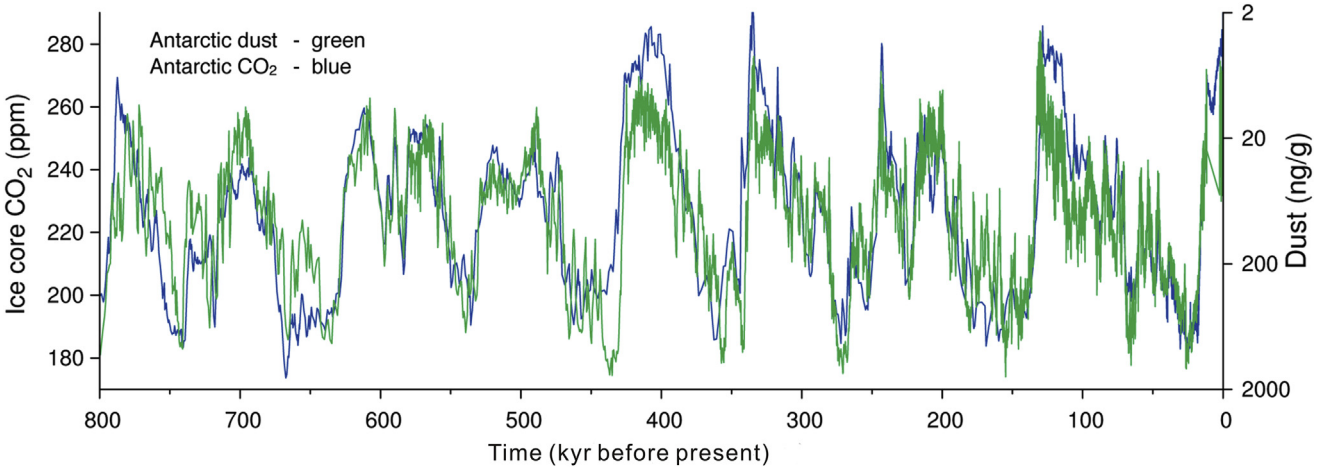

Figure 9. Dust deposition vs. CO_2 concentrations in ppm. The dust plot is inverted and to a logarithmic scale, to reduce amplitude peaks. So dust is closely but inversely correlated to CO_2 concentrations. Source: Epica, 2007.

Please cite this article in press as: Ellis, R., Palmer, M., Modulation of ice ages via precession and dust-albedo feedbacks, Geoscience Frontiers (2016), http://dx.doi.org/10.1016/j.gsf.2016.04.004

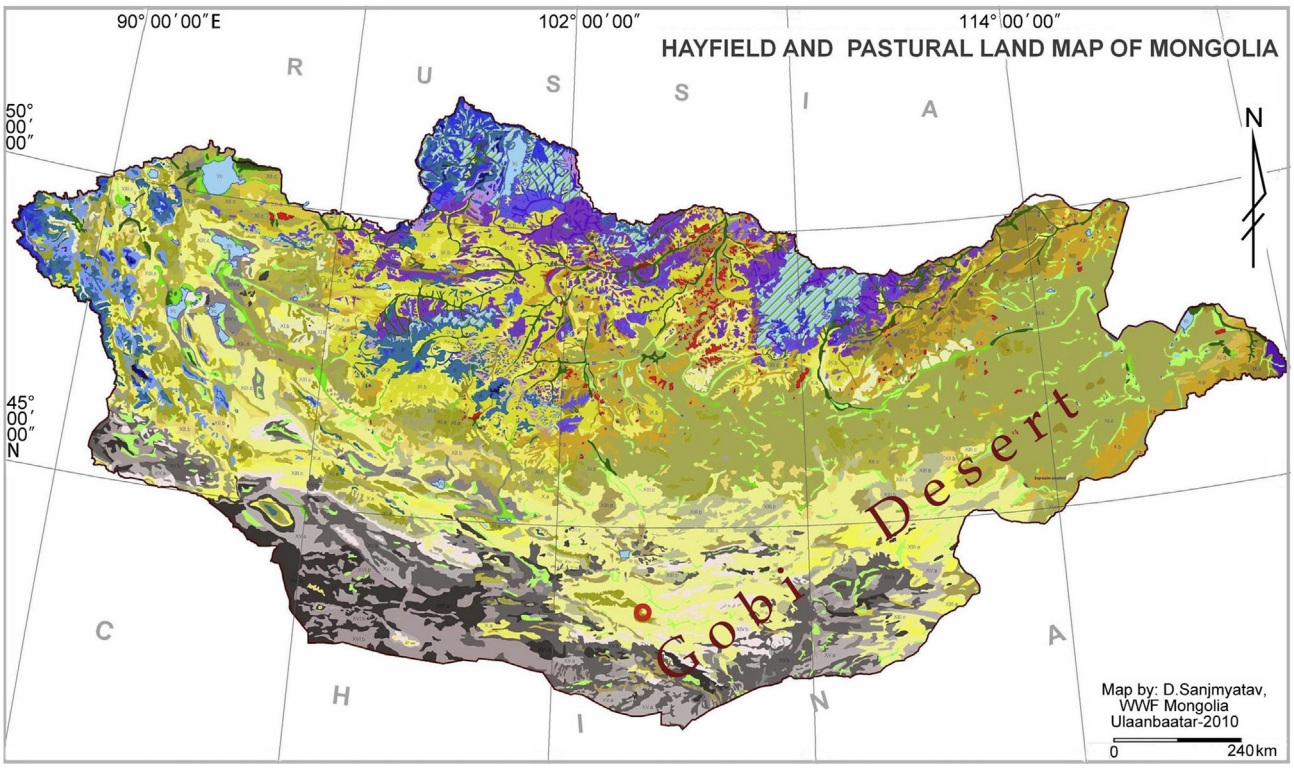

Figure 10. A pastural map of Mongolia. The yellow and green regions mark steppe grasslands, while the greys indicate desert pasture. The town of Dalanzadgad is marked by the red circle. (Image courtesy: WWF Mongolia Maps, Sanjmyatav, D. Tserendash, S.)

from Patagonia to Antarctica have not changed strongly over the last glacial cycles' (Fisher, 2007). A similar situation was found in Greenland, with early investigations suggesting smaller grains and lighter winds during the LGM, while new research has suggested the opposite. But the variation in grain size across the climatic boundary was not particularly significant (Kohfeld and Harrison, 2001; Vallelonga and Svensson, 2014). Larger grain sizes were discovered on the Loess Plateau in China during the LGM, indicating stronger winds there (Jiang et al., 2013), but this did not extend to the northern ice sheets. And if aeolian dust grain sizes in Greenland remain constant, while the transported volume increased by an order of magnitude or more, this would suggest that larger dust sources were the primary cause of increased dust rather than stronger winds.

If increasing aridity and wind were not responsible for the increase in dust, and if CO_2 concentrations are strongly inversely proportional to dust volume, as demonstrated in Fig. 9, the likely candidate for increased dust production has to be CO_2 depletion creating new CO_2 deserts. Especially since dust isotopy indicates that new dust sources were developing at this time. The vast majority of northern China and southern Mongolia lie above 1000 m, while more than a third of this region lies above 1500 m. And while the treelines in Columbia and Brazil only reduced to between 1500 and 2000 m, the environmental conditions in Mongolia are very different. Mongolia is so cold that C_4 grasses would be unable to replace C_3 grasses, as they did in Columbia. And since the moisture demand of C_3 grasses increases substantially as the critical CO_2 partial pressure is approached, they would come under much greater stress in the dry central Asian climate. So even if precipitation levels in this region remained constant across the LGM-Holocene transition, vast swathes of these steppe grasslands would have been decimated by a CO_2 engendered lack of moisture, and vast new CO_2-depletion deserts created at lower altitudes than has been documented in tropical regions.

This has been confirmed by Yu's extensive study of LGM vegetation in central and East Asia, which documents widespread desertification across northern China. The steppe and desert conditions of the Gobi extended south to the 30° parallel and eastwards to the coast, more than quadrupling the extent of this desert and semi-desert region. While the mixed forest treeline was pushed south by 1000 km to the 22° parallel (Yu et al., 2000, 2003). And several more meters of loess deposits were laid down on the Loess Plateau, which extends for some 440,000 km^2 across central China north of Xian and contains loess deposits from all the recent glacial cycles (Jiang et al., 2013). These loess deposits demonstrate that the same regions were generating copious amounts of dust through each glacial cycle, just as the ice-core records from Antarctica also suggest. These deep loess deposits have been interpreted as indicating large reductions in both precipitation (Mahowald, 1999; Petit et al., 1999) and temperature (Tarasov et al., 1999) in Asia during glacial maximums. Tarasov indicated that temperatures in Mongolia were on average between 6 °C and 10 °C colder during the LGM, which is why the PMIP3 map in Fig. 7a displays a localised cold spot centered on Mongolia. Yet just as with the Columbian dry-spot, these localised reductions in temperature and precipitation would not be necessary if CO_2 reductions were the primary cause of upland desertification. It is generally accepted now that western China was actually wetter during the LGM (Yu et al., 2003), but the climatic dichotomy this engenders is often left unexplained.

However, if CO_2 was the primary regulator of desertification in this region then the increase in dust production during the glacial period should be proportional to the land-area above the critical CO_2 extinction altitude. The area above the critical altitude will

Please cite this article in press as: Ellis, R., Palmer, M., Modulation of ice ages via precession and dust-albedo feedbacks, Geoscience Frontiers (2016), http://dx.doi.org/10.1016/j.gsf.2016.04.004

initially be small, only covering a few mountain peaks. But as sea level CO_2 concentrations continue to decrease, the extinction-zone will rapidly widen to include the Chinese and Mongolian plateaus, which range from 1500 m to 1000 amsl. This process will result in a linear decrease in CO_2 concentrations generating an exponential increase in desert lands and dust production, which is exactly what the CO_2 and dust records in Fig. 9 illustrates. This process can be further graphed by using data from the NOAA Global Relief Map (ETOPO1, 2015), and comparing glacial CO_2 concentrations with the land area exposed above the flora extinction-zone. The results can be seen in Fig. 11c and d. The land area subsequently covered by lowering glacial snowlines was also plotted, using snowline data from Porter et al., but the difference generated by reducing snowlines was relatively insignificant (Porter, 2000).

In Fig. 11a, Antarctic dust concentrations were correlated with Antarctic CO_2 deposition over 800 kyr, using Epica3 ice core data. Antarctic data was chosen because it allows the analysis of many glacial cycles, and also because the Greenland CO_2 data is unreliable due to carbonate contamination (Ruth et al., 2007). This trans-polar comparison is justifiable because although Greenland dust levels have a greater amplitude than Antarctic dust, they are coincident and proportional. Fig. 11b plots logarithmic Ngrip Greenland dust (blue) against Epica Antarctic CO_2 (red), demonstrating the same close correlation as seen previously in Fig. 9, which used Antarctic dust data (see also Serno et al., 2015). The correlation between dust and CO_2 in Fig. 11a is surprisingly good, giving an R^2 of ~0.8, indicating a strongly logarithmic inverse dust response to CO_2. This correlation was then plotted against the land area exposed above the critical CO_2 extinction altitude, assuming a minimum sea-level CO_2 concentration of 190 ppm. The effects of low CO_2 on plant survival have already been discussed at length and suggest that the critical CO_2 concentration for plant extinction is between 150 and 170 ppm, depending upon species and other stress factors like moisture. So a variety of plots have been generated using critical CO_2 concentration equivalents between 140 and 170 ppm (140 to 170 μbar), to depict the area of uplands experiencing partial pressures below critical levels as sea level CO_2 concentrations reduce.

The topography of each region will be unique, so two graphs were constructed incorporating global topography and the local topography adjacent to the Gobi Desert, resulting in Fig. 11c and d. The topography determines the form of each plot, with the 170 ppm (170 μbar) plot in Fig. 11d clearly showing the broad highland steppe-lands of northern China and southern Mongolia in the center of the plot, and a much smaller coastal plain at the end. And since these plots also contain a function of time, they are also a graphic representation of an entire ~100 kyr ice-age cycle. The lower left of each graph represents the interglacial period, with high CO_2 concentrations and low dust levels

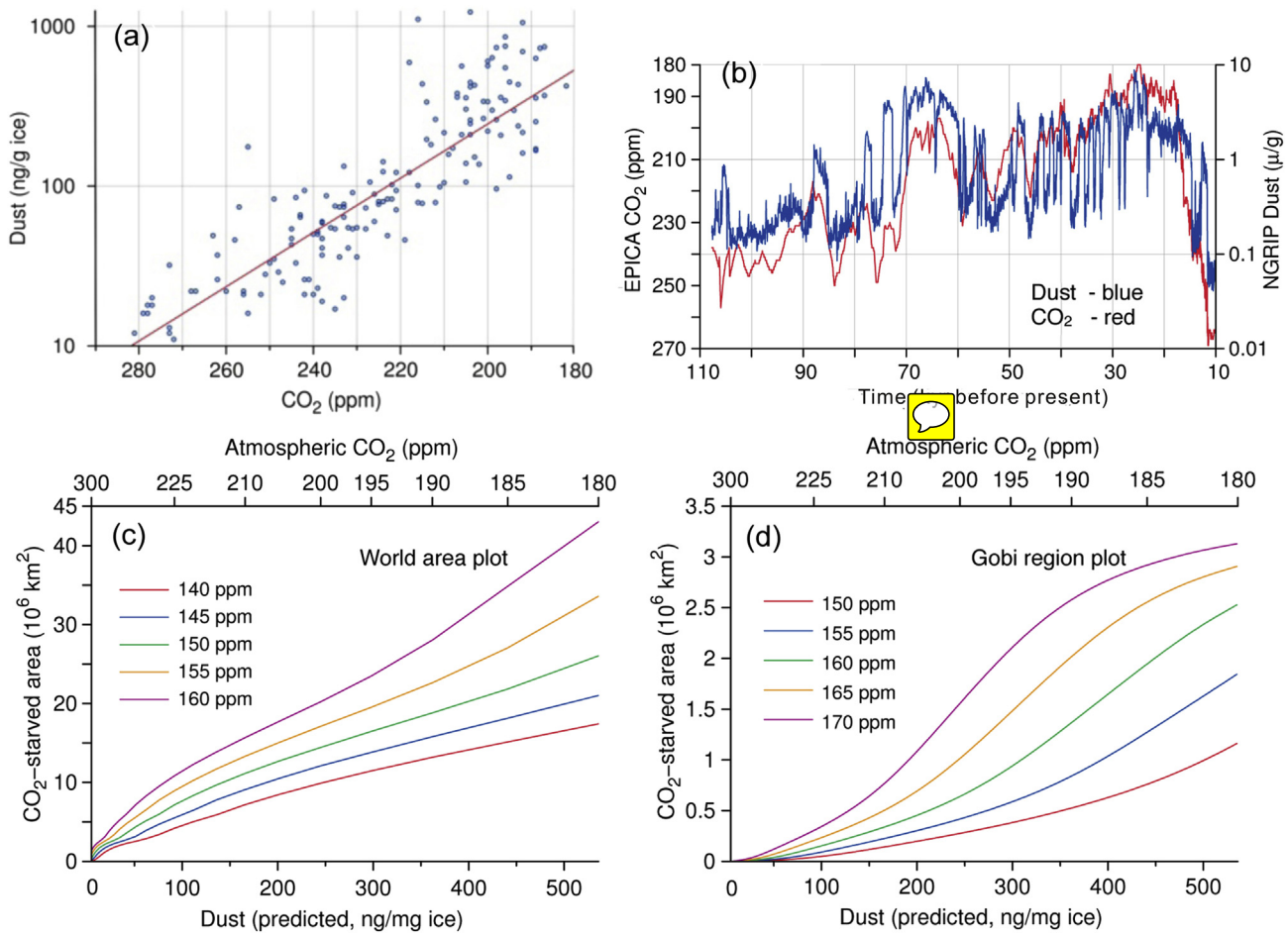

Figure 11. (a) Scatter plot demonstrating the good correlation between CO_2 and dust. Dust on a logarithmic scale. (b) Plot of Greenland dust (blue) vs. Antarctic CO_2 (red), similar to Fig. 9. Dust on a logarithmic scale. Greenland CO_2 data is contaminated and unusable, but Antarctic CO_2 is a viable alternative. (c, d) Two plots of land area above the CO_2 death-zone altitude. Sea-level CO_2 is assumed to be 190 ppm. A range of death-zone CO_2 concentrations are plotted, from 140 to 170 ppm equivalent (140 to 170 μbar). Reduction in atmospheric pressure 50%/5200 m. Area of land above the critical altitude derived from ETOPO1 2015. (c) World land area (CO_2 on a logarithmic scale). (d) The Gobi region land area, 40–50 North & 85–125 East (CO_2 on a logarithmic scale).

Please cite this article in press as: Ellis, R., Palmer, M., Modulation of ice ages via precession and dust-albedo feedbacks, Geoscience Frontiers (2016), http://dx.doi.org/10.1016/j.gsf.2016.04.004

emanating from the well-known moisture deserts. While the upper right corner represents the glacial maximum, with low CO_2 concentrations and high levels of dust generated by the newly created CO_2 deserts. Claussen et al. calculated that world defoliation at the LGM equated to 26×10^6 km^2, as was discussed in Section 5.3, and this would agree well with the land area above the death-zone depicted by the 150 ppm (150 μbar) critical CO_2 concentration in Fig. 11c. Transferring that critical concentration across to Fig. 11d would result in a 1.1×10^6 km^2 increase in desertification for the Gobi region during the LGM. But since plant distress will occur at higher CO_2 concentrations in this region, due to the general lack of moisture, this should be revised up to the 160 ppm (160 μbar) plot line, giving 2.5×10^6 km^2 of new dust source across the Gobi steppe. And the 160 ppm (160 μbar) plot also demonstrates a greater conformity with the CO_2-dust correlation in Fig. 11a.

Since the Gobi steppe is a high plateau, large areas can react near-simultaneously to CO_2 deprivation, creating widespread desertification on very short geological timescales. There are many sudden jumps in the CO_2 concentration record that span 5 ppm in a mater of centuries, and a fall in sea level concentrations from 190 to 185 ppm can lower the high altitude extinction-zone by approximately 150 m. And Fig. 11d indicates that this small decrease will result in a 0.6×10^6 km^2 increase in the Gobi CO_2 desert. So in a matter of a few centuries 600,000 km^2 of new dust sources can be generated – sources that are fresh, previously unscoured, and susceptible to wind erosion. This would result in great dust-storms across Asia and beyond, just as the newly barren lands of North America generated great dust-storms during the 1930s Dust Bowl era. The modern equivalent of Dust Bowl era storm is shown in Fig. 12. And like the Dust Bowl era, these virgin upland Gobi deserts would contain fresh fine dust, rather than the larger sandy grains of an ancient desert, which were easy to transport. Much of this dust settled on the Loess Plateau north of Xian, but many of the lighter fractions settled upon the northern ice sheets, from Alaska and Canada across to northern Greenland and beyond.

5.5. CO_2 and interglacial modulation

This is why the Great Summer that peaked about 170 kyr ago was completely ignored by world temperatures, as can be seen in Fig. 3. Prior to this particular Great Summer there had been insufficient CO_2 reductions and thus no vegetation dieback and no central Asian dust storms to reduce the ice sheet albedo. So the global climate is quite stable at ice-age temperatures, even when subjected to a northern hemisphere high latitude midsummer insolation increase of 80 W/m^2, because the high albedo northern ice sheets can reject the majority of this increased insolation. And so the Great Summer 170 kyr ago provided no global temperature response whatsoever. It was only after the later dust storms, which happened around 150 kyr ago, that that the northern ice sheets were primed and ready for an albedo-assisted Great Summer interglacial warming. And as soon as the next Great Summer increased the insolation upon those dusty ice sheets, the surface temperatures immediately responded and the ice-age ended.

The reasons for the Greenland ice sheet surviving this warming process include its northerly latitude, its high-altitude surface, and the fact that it is located inside a protective bowl surrounded by a ring of low mountains, as can be seen in Fig. 13. In the absence of significant albedo-enhanced forcing and warming feedbacks at this high latitude and altitude, the primary melting and dissipation of an ice sheet will occur at its base, through the normal processes of melting via pressure, friction and geothermal heat, or by ice-sheet spreading and flow. In normal conditions, basal meltwater can flow under pressure into the sea, while the outward flow of ice sheet layers occurs mainly at the base in accordance with the Dansgaard-Johnsen model. At Camp Century, which is close to the coast, the outward flow only starts 900 m down, which represents 65% of the total ice sheet thickness in this region (Dansgaard and Johnsen, 1969). But the bowl formation that underlies the Greenland ice sheet inhibits both meltwater egress and basal spreading. And just as importantly, this mountain-ring also prevents oceanic warming of the ice sheet base, while the base of the adjacent Barents Sea ice sheet was susceptible to oceanic warming and melted (Siegert and

Figure 12. A large dust storm approaches Phoenix Arizona. High winds can move vast quantities of dust, and while the heavier dust particles seen here will soon settle out the finer particles can be transported for thousands of kilometers. Photo courtesy Daniel Bryant.

Please cite this article in press as: Ellis, R., Palmer, M., Modulation of ice ages via precession and dust-albedo feedbacks, Geoscience Frontiers (2016), http://dx.doi.org/10.1016/j.gsf.2016.04.004

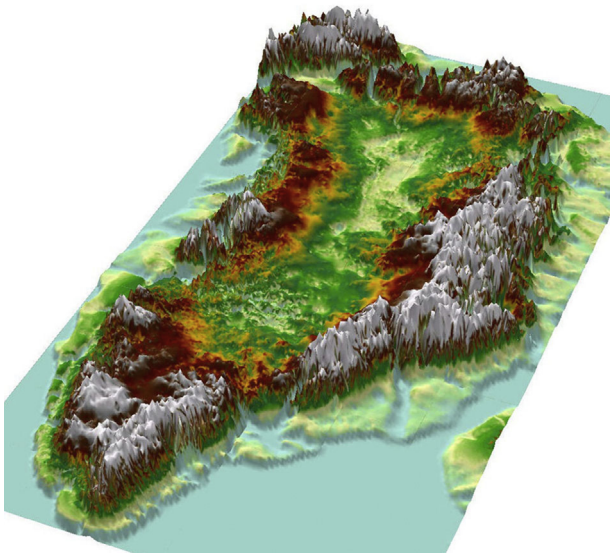

Figure 13. The underlying topography of Greenland, showing the ring of mountains averaging 1200 m high that protect the Greenland ice sheet from melting, flowing or being warmed by the Atlantic. Much of the central valley of Greenland is actually below the modern sea level. Data ETOPO1 Global Relief Model.

Elverhøi, 2002). So the Greenland ice sheet has been captured by topography, isolated from global oceanic warming, and remains a glacial relic in a largely post-glacial world.

So the Earth's long-term climate is almost a bi-stable system incorporating two extremes in temperature: ice-age and interglacial. And interglacial temperatures can be quite stable, as the greatly extended interglacials 430 kyr and 15 kyr ago demonstrate, with the stability of the climate system being maintained at either of these extremes by the thermostatic mechanism of cloud formation (Eschenbach, 2010). But the paleoclimatic record also demonstrates that the preferred regime is the cooler glacial climate, and so even the extended interglacial periods invariably slide back down into cooler glacial conditions. However, while the long ice-age eras are demonstrably very climatically stable, they do have a very prominent Achilles heel – the very strong regional forcing and feedback influences provided by dust and albedo. And this climatic Achilles heel may not only explain all of the interglacial cycles, but also the very rapid and otherwise unexplained Dansgaard-Oeschger (D-O) temperature oscillations – especially if these peculiar temperature spikes involved soot-albedo from conflagrations rather than dust-albedo from barren lands. But that is another story for another day.

6. Summary and conclusions

The primary orbital cycle responsible for interglacial initiation is the precessional Great Summer, which can provide large increases in annual midsummer insolation in the northern hemisphere for several millennia. However, not all Great Summers produce a warming event, while full interglacials only occur every four or five cycles. The additional factor that can achieve this selective regulation is the high albedo of the northern ice sheets, which can reject and reduce the increased insolation of a Great Summer. In order for a Great Summer to generate a significant warming response the northern ice sheets need to be laden with dust, so that the increased insolation can get some leverage on the highly reflective ice. And the mechanism required to achieve this involves surface CO_2 concentrations reducing below 200 ppm, which results in a die-back of high altitude flora, widespread desertification, and dust deposition upon the ice sheets. Fig. 14 depicts all the key elements that play a part in these complex climatic interactions. Note that dust (purple) is only generated once CO_2 (yellow) has reached critically low levels, and that interglacial warming (red) only occurs after dust deposition and when an eccentricity-enhanced Great Summer (dark blue peak) is reached.

The apparent correlation between dust (purple) and eccentricity minima (black) on this graph is merely a function of the eccentricity-enhanced inception of interglacial periods (red peak). An interglacial is only initiated when eccentricity is rising and northern Great Summer Milankovitch insolation is enhanced. Following this temporary warm period, the rate of polar ice regrowth and its associated increase in albedo, controls the cooling-rate of the oceans and climate. These steadily reducing

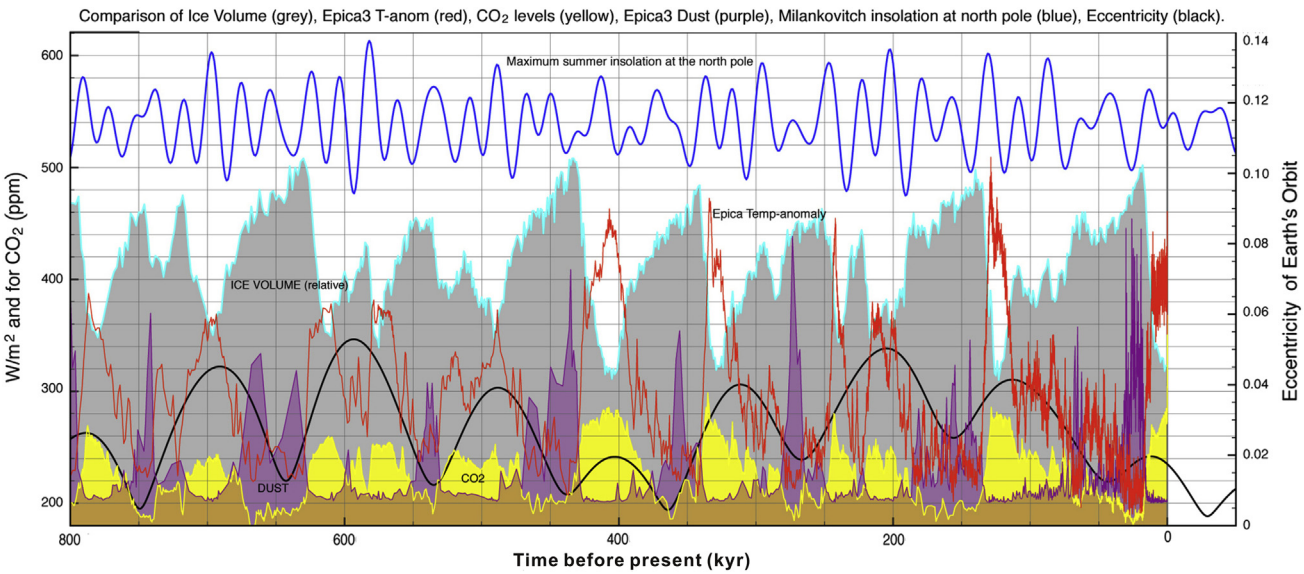

Figure 14. A summary graph of all the factors that play a role in glacial modulation. Key: Ice Volume (grey), Epica3 temperature (red), CO_2 levels (yellow), Epica3 Dust (purple), Laskar Precessional Forcing (blue), Laskar Eccentricity (black). Diagrammatic only - scales adjusted to suit the diagram. Note that there are no strong Great Summers or Great winters for at least 50 kyr into the future, and so the world is unlikely to experience another ice-age for many millennia. Image courtesy of Prof Clive Best.

Please cite this article in press as: Ellis, R., Palmer, M., Modulation of ice ages via precession and dust-albedo feedbacks, Geoscience Frontiers (2016), http://dx.doi.org/10.1016/j.gsf.2016.04.004

temperatures control the equally steady oceanic absorption and sequestration of atmospheric CO_2, which in turn eventually controls the exponential increase in dust production, which then lowers ice-sheet albedo and primes the world for another interglacial warming. Thus one of the primary climatic regulators of interglacial periodicity is the steady rate of increase in polar ice extent. And since it takes about 70 kyr before the ice-sheets are large enough for temperatures and CO_2 to reach a minima, this coincidentally places the increased dust production era close to the next eccentricity minima.

Thus the rate of ice-sheet regrowth plays a key role in determining the ~100 kyr length of the glacial cycle. If temperatures and CO_2 have not reached their critical minimum values before the onset of an eccentricity-enhanced Great Summer, there would be no dust-ice albedo feedbacks. And so the world would wait patiently until the next enhanced Great Summer, when hopefully all the participants in this stand-off between orbital forcing and climate feedbacks are ready to play their part. The glacial world's dust-ice Achilles heel needs to be primed and ready to fire before an interglacial can be fully successful, otherwise the result is merely a 'flash in the pan' – one of the many minor warming events of no consequence in the paleoclimatic record. In which case, interglacial warming is eccentricity and polar ice regrowth regulated, Great Summer forced, and dust-ice albedo amplified. And the greenhouse-gas attributes of CO_2 play little or no part in this complex feedback system.

Acknowledgements

I would like to thank Prof. Michael Palmer for his tireless efforts in mentoring this paper. Prof. Palmer performed data analysis, prepared graphics, and critiqued the paper at each stage of its development. The paper would not have reached the standard achieved, without his enthusiasm and expertise. Thanks also to Prof. Clive Best, who supplied the summary graphic in Fig. 14.

References

Abe-Ouchi, A., Saito, F., Kawamura, K., Raymo, M.E., Okuno, J.I., Takahashi, K., Blatter, H., 2013. Insolation-driven 100,000-year glacial cycles and hysteresis of ice-sheet volume. Nature 500 (7461), 190–193.

Bakker, J., et al., 1990. Tectonic and Climatic Controls on Late Quaternary Sedimentary Processes in a Neotectonic Intramontane Basin, the Pitalito Basin, South Colombia. Department of Soil Science, University of Wagenigen, Netherlands, ISBN 90-9003479-X. SISO am-colo 565 UDC [552.5:627.81] (861) (043.3) See p.133.

Bateman, M.D., Murton, J.B., 2006. The chronostratigraphy of late pleistocene glacial and periglacial aeolian activity in the Tuktoyaktuk Coastlands, NWT, Canada. Quaternary Science Reviews 25 (s 19–20), 2552–2568.

Behling, H., 1997. Late Quaternary vegetation, climate and fire history from the tropical mountain region of Morro de Itapeva, SE Brazil. Palaeogeography Palaeoclimatology Palaeoecology 129, 407–422.

Bory, A.J., 2014. A 10,000 km Dust Highway between the Taklamakan Desert and Greenland.

Bouttes, N., Paillard, D., Roche, D.M., 2010. Impact of brine-induced stratification on the glacial carbon cycle. Climate of the Past 6 (5), 575–589.

Campion, N., Dally, A., 1997. The Great Year: Astrology, Millenarianism and History in the Western Tradition. The Great Year: Astrology, Millenarianism, and History in the Western Tradition. Arkana.

Claussen, M., Selent, K., Brovkin, V., Raddatz, T., 2012. Impact of Co_2 and climate on Last Glacial Maximum vegetation – a factor separation. Biogeosciences Discussions 10 (6), 3593–3604.

CLIMAP Project Members, 1976 & 1981. Seasonal Reconstruction of the Earth's Surface at the Last Glacial Maximum. Geological Society of America Map and Chart Series MC-36, Pangaea Data Publisher, Boulder, Colorado. https://doi.pangaea.de/10.1594/PANGAEA.64426.

Climate Temperatures, 2014. http://www.climatemps.com.

Cuffey, K.M., Clow, G.D., 1997. Temperature, accumulation and ice sheet elevation in central Greenland through the last deglacial transition. Journal of Geophysical Research Atmospheres 102 (C12), 26383–26396.

Dansgaard, W., Johnsen, S.J., 1969. A flow model and a time scale for the ice core from camp century, Greenland. Journal of Glaciology 8 (53), 215–223.

Delmonte, B., Basile-Doelsch, I., Petit, J.R., Maggi, V., Revel-Rolland, M., Michard, A., Jagoutz, E., Grousseth, F., 2004. Comparing the EPICA and Vostok dust records during the last 220,000 years: stratigraphical correlation and provenance in glacial periods. Earth-Science Reviews 66 (1–2), 63–87.

Dyke, A.S., Andrews, J.T., Clark, P.U., England, J.H., Miller, G.H., Shaw, J., Veillettea, J.J., 2010. The Laurentide and Innuitian ice sheets during the Last Glacial Maximum. Quaternary Science Reviews 21 (1), 9–31.

Elias, S.A., Brigham-Grette, J., 2013. Late Pleistocene Glacial Events in Beringia. Encyclopedia of Quaternary Science, pp. 191–201.

Eschenbach, W., 2010. The thunderstorm thermostat hypothesis: how clouds and thunderstorms control the earth's temperature. Energy & Environment 21 (4), 201–216.

ETOPO1 Global Relief Model NOAA. National Center for Environmental Information https://www.ngdc.noaa.gov/mgg/image/fig1_global_histogram.png.

Fenton, M., Schreiner, B., Neilson, E., et al., 1994. Quaternerary Geology of the Western Plains. Geological Atlas of the Western Canada Sedimentary Basin. fig 26.7. Alberta Research Council, Edmonton.

Fischer, H., Fundel, F., Ruth, U., Twarloh, B., Wegner, A., Udisti, R., Becagli, B., Castellano, E., Morganti, A., Severi, M., Wolffc, E., Littot, G., Röthlisberger, R., Mulvaney, R., Hutterli, M.A., Kaufmann, P., Federer, U., Lambert, F., Bigler, M., Hansson, M., Jonsell, U., Angelis, M., Boutron, C., Siggaard-Andersen, M., Steffensen, J.P., Barbante, C., Gaspari, V., Gabrielli, P., Wagenbach, D., 2007. Reconstruction of millennial changes in dust emission, transport and regional sea ice coverage using the deep Epica ice cores from the Atlantic and Indian Ocean sector of Antarctica. Earth and Planetary Science Letters 260 (1–2), 340–354.

Ganopolski, A., Calov, R., 2011. The role of orbital forcing, carbon dioxide and regolith in 100 kyr glacial cycles. Climate of the Past Discussions 7 (4), 1415–1425.

Ganopolski, A., Calov, R., Claussen, M., 2010. Simulation of the last glacial cycle with a coupled climate ice-sheet model of intermediate complexity. Climate of the Past 5 (2), 229–244.

Gerhart, L.M., Ward, J.K., 2010. Plant responses to low [CO_2] of the past. New Phytologist 188 (3), 674–695.

Goldblatt, C., Watson, A.J., 2012. The runaway greenhouse: implications for future climate change, geoengineering and planetary atmospheres. Philosophical Transactions of the Royal Society A Mathematical Physical & Engineering Sciences 370 (1974), 4197–4216.

Goldblatt, C., Robinson, T.D., Zahnle, K.J., Crisp, D., 2014. Corrigendum: low simulated radiation limit for runaway greenhouse climates. Nature Geoscience 7 (6), 661–667.

Hansen, J., et al., 2011. Storms of My Grandchildren. Bloomsbury, New York.

Hansen, J., Sato, M., et al., 2012. Climate Sensitivity Estimated from Earth's Climate History, p. 7 fig 5. NASA Goddard Institute for Space Studies.

Harlow, R.C., Burke, E.J., Scott, R.L., Shuttleworth, W.J., Brown, C.M., Petti, J.R., 2004. Derivation of temperature lapse rates in semi-arid south-eastern Arizona. Hydrology & Earth System Sciences 8 (6), 1179–1185.

Hooghiemstra, H., Van der Hammen, T., 2004. Quaternary Ice-Age dynamics in the Colombian Andes: developing an understanding of our legacy. Philosophical Transactions 359, 173–181. http://dx.doi.org/10.1098/rstb.2003.1420.

Huybers, P., 2006. Early Pleistocene glacial cycles and the integrated summer insolation forcing. Science 313 (5786), 508–511.

IPCC AR4, 2007. Paleoclimate B6.1 Orbital Forcing p. 445 & FAQ 6.1 What Caused the Ice Ages p. 449.

IPCC AR5, 2013. Information from Paleoclimate Archives 5.2.1.1, p. 388.

Jiang, W., Cheng, Y., Yang, X., Yang, S., 2013. Chinese Loess Plateau vegetation since the Last Glacial Maximum and its implications for vegetation restoration. Journal of Applied Ecology 50 (2), 440–448.

Johnson, M., et al., 2005. Climate-independent paleoaltimetry using stomatal density in fossil leaves as a proxy for CO2 partial pressure. Geology 33 (1), e82–e83. http://dx.doi.org/10.1130/0091-7613-33.1.e82.

Jolly, D., Haxeltine, A., 1997. Effect of low glacial atmospheric Co_2 on tropical African Montane vegetation. Science 276 (5313), 786–788.

Kirkby, J., Mangini, A., Muller, R.A., 2004. The glacial cycles and cosmic rays. Earth and Planetary Science Letters.

Kohfeld, K.E., Harrison, S.P., 2001. Dirtmap: the geological record of dust. Earth-Science Reviews 54 (1–3), 81–114.

Körner, C., Paulsen, J., 2004. A world-wide study of high altitude treeline temperatures. Journal of Biogeography 1 (31), 713–732.

Körner, C., et al., 2010. Alpine Plant Life: Functional Plant Ecology of High Mountain Ecosystems. ISBN-13: 978–3540003472.

Krinner, G., Boucher, O., Balkanski, Y., 2006. Ice-free glacial northern Asia due to dust deposition on snow. Climate Dynamics 27 (6), 613–625.

Kuhle, M., 1988. The Pleistocene glaciation of Tibet and the onset of ice ages — an autocycle hypothesis. Geojournal 17 (4), 581–595.

Lambert, F., Kug, J.-S., Park, R.J., Mahowald, N., Winckler, G., Abe-Ouchi, A., Lambert, F., Kug, J.S., Park, R.J., Mahowald, N., Winckler, G., Abe-Ouchi, A., O'ishi, R., Takemura, T., Lee, J.-H., 2013. The role of mineral-dust aerosols in polar temperature amplification. Nature Climate Change 3 (5), 487–491.

Laskar, J., Joutel, F., Boudin, F., et al., 2004. The Institut de mecanique celeste et de calcul des ephemerides. VO Solar System Portal IMCCE Paris Data Center.

Lisiecki, L.E., 2010. Links between eccentricity forcing and the 100,000-year glacial cycle. Nature Geoscience 3 (5), 349–352.

Liu, H.S., 1998. Glacial-interglacial changes induced by pulse modulation of the incoming solar radiation. Journal of Geophysical Research Atmospheres 1032 (D20), 26147–26164.

Please cite this article in press as: Ellis, R., Palmer, M., Modulation of ice ages via precession and dust-albedo feedbacks, Geoscience Frontiers (2016), http://dx.doi.org/10.1016/j.gsf.2016.04.004

Mahowald, N., Karen, K., Margaret, H., Yves, B., Harrison, S.P., Colin, P.I., Schulz, M., Rodhe, H., 1999. Dust sources and deposition during the Last Glacial Maximum and current climate: a comparison of model results with Paleodata from ice cores and marine sediments. Journal of Geophysical Research Atmospheres 104, 895–915.

Mahowald, N.M., Muhs, D.R., Levis, S., Rasch, P.J., Yoshioka, M., Zender, C.S., Luo, Chao, 2006. Change in atmospheric mineral aerosols in response to climate: last glacial period, preindustrial, modern, and doubled carbon dioxide climates. Journal of Geophysical Research Atmospheres 111 (D10), 1879–1894.

McElwain, J.C., 2004. Climate-independent Paleoaltimetry using stomatal density in fossil leaves as a proxy for CO_2 partial pressure. Geology 32 (12), 1017–1020.

McGee, D., Wallace, S., et al., August 2010. Gustiness: the driver of glacial dustiness. Quaternary Science Reviews 29 (17), 2340. http://dx.doi.org/10.1016/j.quascirev.2010.06.009.

Moore, R., Clarke, W., Vodopich, D., 1995. Botany: Plant Diversity. ISBN 978–0697037756.

Muhs, D.R., Prospero, J.M., Baddock, M.C., Gill, T.E., Sept 2014. Identifying sources of Aeolian mineral dust: present and past. Mineral dust- a key player in the earth system. Research Gate. http://dx.doi.org/10.1007/978-94-017-8978-3__3.

Muller, R., MacDonald, G., 1997. Spectrum of 100-kyr glacial cycle: orbital inclination, not eccentricity. P.N.A.S 94 (16), 8329.

NOAA NCDC National Center for Environmental Information Station number 44373, Dalanzadgad. FTP data link www://ftp://ftp.atdd.noaa.gov/pub/GCOS/WMO-Normals/RA-II/MO/44373.TXT.

OCO-2, 2015. Orbiting Carbon Observatory 2. NASA CO_2 images. NASA CO_2 model simulation video.

Osborne, C.P., Beerling, D.J., 2005. Nature's green revolution: the remarkable evolutionary rise of C4 plants. Philosophical Transactions of the Royal Society of London 361 (1465), 173–194.

Petit, J.R., Jouzel, J., Raynaud, D., Barkov, N.I., Barnola, J.M., Basile, I., Bender, Chappellaz, J., Davis, M., Delaygue, G., Delmotte, M., Kotlyakov, V.M., Legrand, M., Lipenkov, V.Y., Lorius, C., PÉpin, L., Ritz, C., Saltzman, E., Stievenard, M., 1999. Climate and atmospheric history of the past 420,000 years from the Vostok ice core, Antarctica. Nature 399 (6735), 429–436.

Pinto, H., Sharwood, R.E., Tissue, D.T., Ghannoum, O., 2014. Photosynthesis of C^3, C^3–C^4, and C^4 grasses at glacial CO_2. Journal of Experimental Botany 65 (13), 271–278.

PMIP3, 2015. Paleoclimate Modeling Intercomparison Project (PMIP3) Link to precipitation map, an average of eleven models: http://pmip3.lsce.ipsl.fr/share/database/maps/lgm/pr_ann_piControl_diff_lgm_AverageModel.png. Link to temperature map, an average of eleven models: http://pmip3.lsce.ipsl.fr/share/database/maps/lgm/tas_ann_piControl_diff_lgm_AverageModel.png.

Porter, S.C., 2000. Snowline depression in the tropics during the last glaciation. Quaternary Science Reviews 20 (10), 1067–1091.

Rind, D., Peteet, D., 1985. Terrestrial conditions at the Last Glacial Maximum and climap sea-surface temperature estimates: are they consistent? Quaternary Research 24 (1), 1–22.

Roberts, S.P., Elekonich, M.M., 2005. Muscle biochemistry and the ontogeny of flight capacity during behavioral development in the honey bee, *Apis Mellifera*. Journal of Experimental Biology 208 (22), 4193–4198.

Ruth, U., Bigler, M., et al., 2007. Dust concentration in the NGRIP ice core. Geophysical Research Letters 34 (3). http://dx.doi.org/10.1029/2006GL027876. Pangaea NGRIP data resource doi:10.1594/PANGAEA.587836.

Serno, S., Winckler, G., Anderson, R.F., Maier, E., Ren, H., Gersonde, R., Haug, G.H., 2015. Comparing dust flux records from the subarctic north Pacific and Greenland: implications for atmospheric transport to Greenland and for the application of dust as a chronostratigraphic tool. Paleoceanography 30 (6), 681–688.

Shi, Z., Haworth, M., Feng, Q., Cheng, R., Centritto, M., 2015. Growth habit and leaf economics determine gas exchange responses to high elevation in an evergreen tree, a deciduous shrub and a herbaceous annual. AoB Plants 7.

Siegert, M.J., Elverhøi, A., 2002. The Eurasian Arctic during the Last Ice Age: a vast ice sheet once covered the Barents Sea. Its sudden disappearance 100 centuries ago provides a lesson about western Antarctica today. American Scientist 97 (1), 32–39.

Still, C.J., Berry, J.A., Collatz, G.J., Defries, R.S., 2003. Global distribution of C^3, and C^4, vegetation: carbon cycle implications. Global Biogeochemical Cycles 17 (1), 1006.

Svensson, A., Biscaye, P.E., Grousset, F.E., 2000. Characterization of late glacial continental dust in the Greenland ice core project ice core. Journal of Geophysical Research Atmospheres 105 (27), 4637–4656.

Svensson, J., Virkkula, A., Meinander, O., Kivekäs, N., Hannula, H.R., Järvinen, O., Peltoniemi, J.I., Gritsevich, M., Heikkilä, A., Kontu, A., Hyvärinen, A.-P., Neitola, K., Brus, D., Dagsson-Waldhauserova, P., Anttila, K., Hakala, T., Kaartinen, H., Vehkamäki, M., de Leeuw, G., Lihavainen, H., 2015. Soot on snow experiments: light-absorbing impurities effect on the natural snowpack. Cryosphere Discussions 9 (1), 1227–1267.

Tarasov, P.E., Peyron, O., Guiot, J., Brewer, S., Volkova, V.S., Bezusko, L.G., Dorofeyuk, Kvavadze, E.V., Osipova, I.M., Panova, N.K., 1999. Last Glacial Maximum climate of the former Soviet Union and Mongolia reconstructed from pollen and plant macrofossil data. Climate Dynamics 15 (3), 227–240.

Taylor, K., Alley, R., et al., 1997. NOAA National Climatic Data Center, Online Files GISP2 Ice Core 110 KYr Electrical Conductivity Measurements.

Terashima, I., Yokoi, Y., 1995. Is photosynthesis suppressed at higher elevations due to low CO_2, pressure? Ecology 76 (8), 2663–2668.

Vallelonga, P., Svensson, A., 2014. Ice Core Archives of Mineral Dust. Springer, Netherlands, pp. 463–485.

Ward, J.K., Harris, J.M., Cerling, T.E., Wiedenhoeft, A., Lott, M.J., Dearing, M.D., Coltrain, J.B., Ehleringer, J.R., 2005. Carbon starvation in glacial trees recovered from the la brea tar pits, southern California. Proceedings of the National Academy of Sciences of the United States of America 102 (3), 690–694.

Warren, S., et al., 2009. Black Carbon in Arctic Snow and its Effect on Surface Albedo Pacific Northwest National Laboratory, Nov 2009.

Warren, S.G., 1984. Review impurities in snow: effects on albedo and snowmelt. Annals of Glaciology 5, 177–179.

Willie, M., Hoogheimstra, H., et al., 2001. Environmental Change in the Colombian Subandean Forest Belt From 8 Pollen Records: The Last 50 kyr.

Willie, M., et al., 2000. Paleoenvironmental history of the Popayán area since 27 000 yr BP at Timbio. Review of Palaeobotany and Palynology 109 (1), 45–63. http://dx.doi.org/10.1016/S0034-6667(99)00047-0.

Woillez, M.N., Kageyama, M., Krinner, G., Noblet-Ducoudré, N.D., Viovy, N., Mancip, M., 2011. Impact of CO_2 and climate on the Last Glacial Maximum vegetation: results from the orchidee/ipsl models. Climate of the Past 7 (2), 557–577.

Wu, H.B., Guiot, J., Brewer, S., Guo, Z.T., Peng, C.H., 2007. Dominant factors controlling glacial and interglacial variations in the treeline elevation in tropical Africa. Proceedings of the National Academy of Sciences of the United States of America 104 (23), 9720–9724.

Yoke, H., 1985. Li, Qi and Shu: An Introduction to Science and Civilization in China. Precession calculated to be 18 kyr. ISBN: 978-0486414454. http://www.amazon.com/Li-Qi-Shu-Introduction-Civilization/dp/0486414450.

Yu, G., Chen, X., Ni, J., Cheddadi, R., Guiot, J., Han, H., Harrison, S.P., Huang, C., Ke, M., Kong, Z., Li, S., Li, W., Liew, P., Liu, G., Liu, J., Liu, Q., Liu, K.-B., Prentice, I.C., Qui, W., Ren, G., Song, C., Sugita, S., Sun, X., Tang, L., Van Campo, E., Xia, Y., Xu, Q., Yan, S., Yang, X., Zhao, J., Zheng, Z., 2000. Palaeovegetation of china: a pollen data-based synthesis for the mid-Holocene and Last Glacial Maximum. Angewandte Chemie 27 (3), 635–664.

Yu, G., Xue, B., Liu, J., Chen, X., 2003. Lgm lake records from china and an analysis of climate dynamics using a modelling approach. Global & Planetary Change 38 (s 3–4), 223–256.

Please cite this article in press as: Ellis, R., Palmer, M., Modulation of ice ages via precession and dust-albedo feedbacks, Geoscience Frontiers (2016), http://dx.doi.org/10.1016/j.gsf.2016.04.004